2023

Advances in Precision Microfabrication Through Digital Light Processing: System Development, Material and Applications

Xinhui Wang
University College Dublin, Ireland

Jinghang Liu
Technological University Dublin, Ireland, jinghang.liu@tudublin.ie

Yang Zhang
Technological University of Denmark, Kgs. Lyngby, Denmark

See next page for additional authors

Recommended Citation

Authors

Xinhui Wang, Jinghang Liu, Yang Zhang, Per Magnus Kristiansen, Aminul Islam, Michael Gilchrist, and Nan Zhang
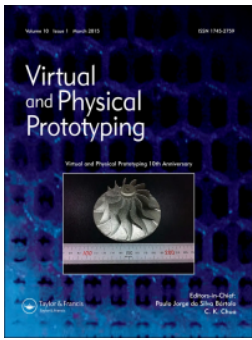
Advances in precision microfabrication through digital light processing: system development, material and applications

Xinhui Wang, Jinghang Liu, Yang Zhang, Per Magnus Kristiansen, Aminul Islam, Michael Gilchrist & Nan Zhang

Published online: 24 Aug 2023.

Submit your article to this journal ⬈

Article views: 610

View related articles ⬈

View Crossmark data ⬈

Taylor & Francis
Taylor & Francis Group

REVIEW ARTICLE

OPEN ACCESS | Check for updates

Advances in precision microfabrication through digital light processing: system development, material and applications

Xinhui Wang[a], Jinghang Liu[b], Yang Zhang[c], Per Magnus Kristiansen[a,d], Aminul Islam[c], Michael Gilchrist[a] and Nan Zhang[a]

[a]Centre of Micro/Nano Manufacturing Technology (MNMT-Dublin), School of Mechanical & Materials Engineering, University College Dublin, Dublin, Ireland; [b]School of Mechanical Engineering, Technological University Dublin, Dublin, Ireland; [c]Department of Civil and Mechanical Engineering, Technical university of Denmark, Kgs. Lyngby, Denmark; [d]School of Engineering, Institute of Polymer Nanotechnology (INKA), FHNW University of Applied Sciences and Arts Northwestern Switzerland Windisch, Switzerland

ABSTRACT

Digital Light Processing (DLP) is an advanced additive manufacturing technology which has garnered substantial recognition and has been extensively applications in various fields. This review focuses on the precision microfabrication process of DLP, providing an overview of the DLP 3D printing system, including the digital light engine, project lenses, motorised stage and resin vat for micro-structure fabrication. Additionally, this review paper comprehensively analyses commercially available DLP printers, covering resolution, cost and a detailed discussion on the importance of photopolymer resins, emphasising the monomer, photo-initiator, photo-absorber, etc. Based on the photopolymerisation theory, the DLP high-precision printing process is analysed, which is critical for producing complex microstructures. It also briefly discusses the application of DLP microfabrication including microfluidic chip printing. Finally, this paper summarises the advanced trends and challenges of DLP printing in high-precision, large-area, multi-material and high-speed printing; and it provides an in-depth understanding of DLP technology, highlighting its potential for various applications and addressing challenges that need to be overcome in future research.

1. Introduction

Additive manufacturing (AM), narrowly speaking as 3D printing, is a rapidly emerging technology for constructing sophisticated geometric features and structures by depositing or photocuring materials. Precision fabrication of three-dimensional structures with high integrity and fidelity is achieved through 3D printing. This computer-controlled AM technique eliminates the need for moulds, as commonly used in traditional subtractive manufacturing and forming methods. This technique involves the layer-by-layer addition of materials guided by computer-aided design (CAD), resulting in a highly accurate and robust end product. Various 3D printing methods have emerged and become available with AM technology and material development. Figure 1 shows several widely adopted 3D printing technologies, including fused deposition modelling (FDM), direct ink writing (DIW), inkjet printing (Ink-jet), two-photon polymerisation (TPP) and vat photopolymerisation, such as DLP and stereolithography (SLA). Among these techniques, only

a few 3D printing techniques utilise localised photopolymerisation to achieve high-resolution microfabrication of 3D structures. These technologies include SLA, DLP and TPP. SLA selectively polymerises a liquid polymer resin with a rastering laser layer-by-layer manner to cause localised polymerisation and solidification until a solid 3D object is produced [1]. Its printing resolution is approximately 100 μm [2]. DLP has its roots in SLA and employs a process of localised photo-curing, which involves projecting 2D patterns onto the surface of a liquid polymer resin, achieving single-micron resolution with a centimetre-level printing area, using Digital Micro-mirror Devices (DMD) and high-precision displacement stages. TPP achieves the highest spatial resolution (down to 100 nm) in the AM field by utilising an ultrafast pulsed laser to generate a high flux of photons within a small temporal and spatial window.

Localised photopolymerisation technology has become more widespread during the past decade, with printing resolution being a critical quality indicator of 3D printing. Compared to extrusion-based and inkjet-

CONTACT Nan Zhang ✉ nan.zhang@ucd.ie 🖃 Centre of Micro/Nano Manufacturing Technology (MNMT-Dublin), School of Mechanical & Materials Engineering, University College Dublin, Dublin 4, Ireland
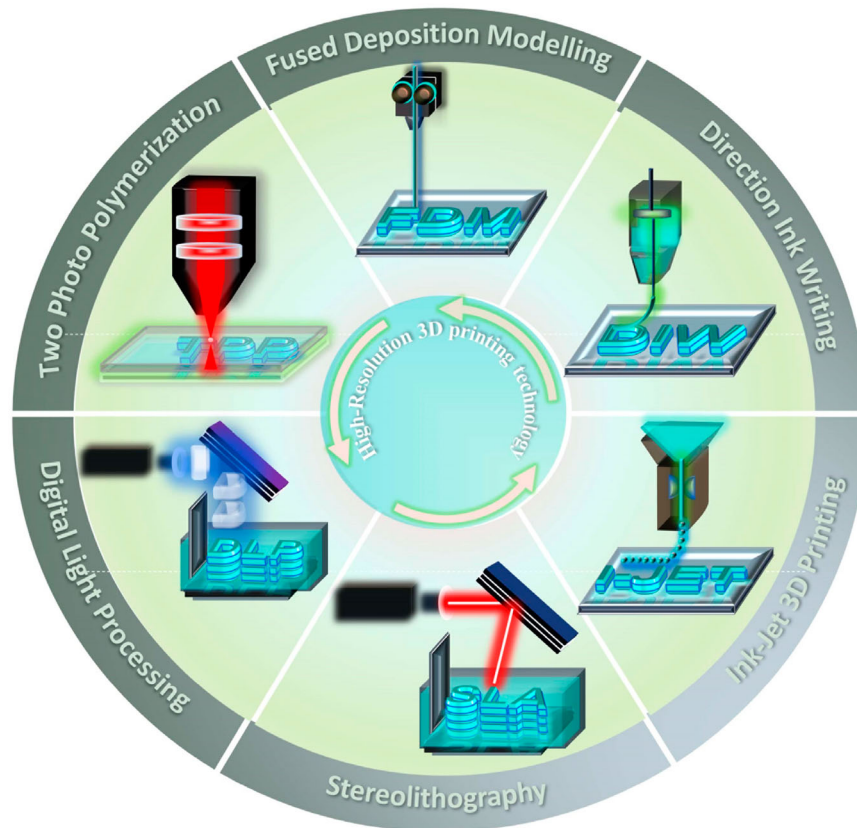
Figure 1. Conventional AM printing techniques.

based 3D printing technologies, DLP offers significant advantages in high printing resolution, with resolutions as low as a single micrometre, and mild working conditions. Notably, SLA is the photocuring 3D printing technique that can print large structures [3]. However, compared with DLP and TPP, SLA has a low print resolution [4], which is currently used to print large structures with a precision of around 100 μm. As the highest precision photocuring 3D printing technology available, TPP can print below 200 nm or close to the diffraction limit [5]. However, the print speed of TPP is slow, with a printing rate of 1–20 cubic millimetres per hour, and is typically used to make millimetre-scale objects [6]. Compared to SLA and TPP, DLP technology excels in print resolution, width and speed. DLP achieves a remarkable single-micron resolution and larger and more complex designs with its centimetre-scale print width of 70–100 mm/h print speeds, ensuring efficient production.

This review paper highlights high-precision microfabrication using DLP. First, the history of DLP over the past 30 years is outlined, followed by a summary of hardware system component development and an explanation of how sub-hardware systems affect the final printing accuracy of DLP. The review comprehensively elucidates the working principle and corresponding mathematical model based on the photopolymer resin of DLP. Based

on printing resolution, this review systematically summarises some prominent companies currently on the market with their corresponding classic commercial DLP 3D printers. Next, the common photopolymer resin compositions currently on the market (monomer, photo-initiator, photo-absorber, etc.) are summarised. The impact of distinct process parameters and material ratios on the mechanical characteristics of the printed structure is analysed and elucidated. The review then proposes applications that rely on DLP technology precision microfabrication. Furthermore, based on high precision, large area, multi-materials and high-speed printing, some perspectives of DLP towards high-precision microfabrication are provided. Finally, the article concludes and proposes some viewpoints and challenges regarding the directions of DLP for precision microfabrication.

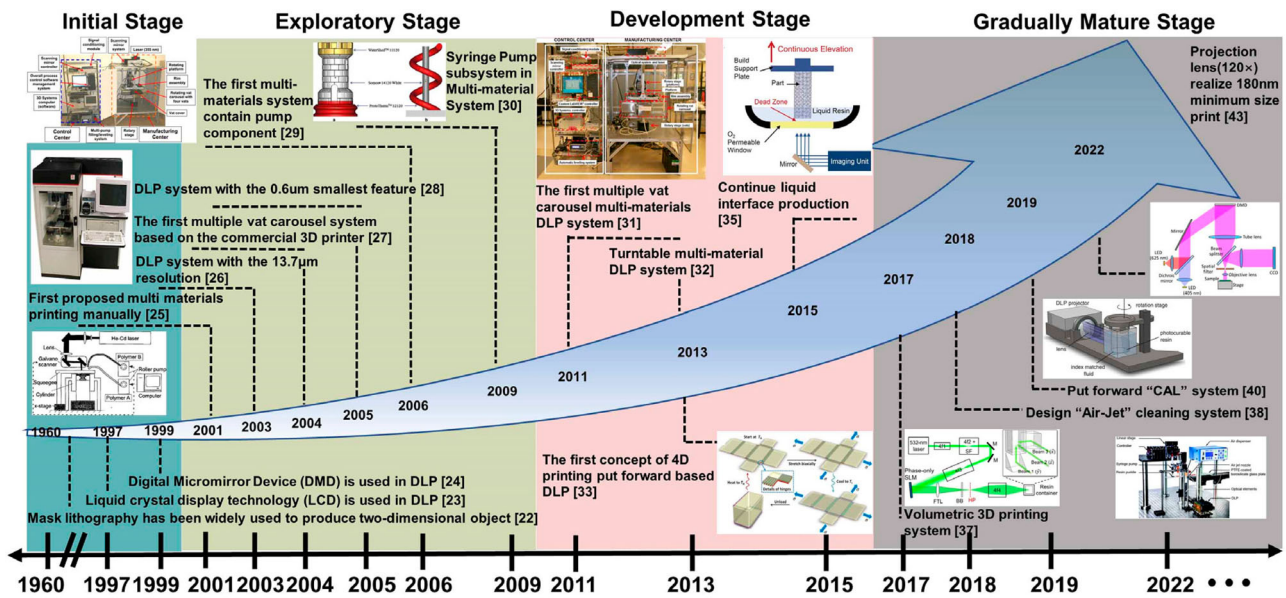## 2 Historical evolutions of DLP

In the 1960s, with the rapid development of the 'Integrated Circuit' (IC) industry, mask lithography technology was used widely to create two-dimensional objects [4]. In 1986, Charles Hull [7] acquired a patent based on aggregating a series of individual cross-section images to fabricate 3D structures using a computer-controlled light beam, and he founded his own 3D

printing company called '3D Systems'. The same year, Larry Hornbeck of Texas Instruments (TI) patented DLP technology, which first comprehensively describes the DMD chip [8]. The late 1980s and early 1990s were dynamic times when significant steps were made in commercialising DLP technology by big companies such as 3D Systems, Quadrax, Mitsubishi Heavy Industries, DuPont, etc. In 1997, Bertsch et al. first proposed layer-by-layer printing using liquid crystal display technology (LCD) to generate dynamic layer patterns [9]. However, the low-resolution contrast ratio makes DMD more suitable for DLP than LCD. Therefore, in 1998, Laurence et al. attempted to use DMD to replace the LCD for the DLP printing system [10]. Figure 2 outlines the historical development of DLP technology.

During the twenty-first century, the development of DLP technology has continued apace. A fundamental challenge is how to achieve multiple materials. In 2001, Maruo et al. [11] first proposed manually replacing the resin tank to realise multi-materials printing. This unprecedented attempt to open a new area attracted numerous scientists to multi-material printing. In 2003, Hadipoespito et al. [12] successfully developed a high-resolution DLP printing system (up to 13.7 μm). In 2004, Wicker et al. [13] designed a multiple-vat carousel system based on a commercial 3D printer (3D systems 250/50SL) to achieve multi-materials printing. To improve printing resolution, in 2005, Sun et al. [14] used the DMD as the dynamic mask to design the early-version projection micro stereolithography (PμSL) system with 0.6 μm resolution. In 2006, Asim and Wicker [13], inspired by the extrusion-based 3D printing system, modified the rotating vat and added a multi-pump filling/levelling system to get a new multi-material system. In 2009, Jae and Wicker [15] proposed a novel printing system capable of producing complex structures with multiple materials, which includes a syringe pump subsystem to control material dispensing into the build vat. In 2011, Jae and Wicker [16] introduced a rotating vat carousel system for 3D printing. To optimise printing efficiency, they developed a custom LabVIEW control system that automated the entire process. As technology patents expired around 2010, many low-cost DLP printers entered the market. With the popularisation of funding platforms like Kickstarter, some companies like B9 Creator (2012) received funding and produced affordable devices priced under 3000 USD based on DLP technology [17].In 2013, Zhou et al. [18] added polydimethylsiloxane (PDMS) film to the bottom glass to reduce the adhesive interaction force, improving printing accuracy and efficiency. At the same time, Qi et al. [19] proposed 4D printing based on DLP. They used the glassy shape memory

polymer fibres to print sophisticated structures and spatially varying curvature. When the temperature changes, the shapes of 3D structures will correspondingly. In 2014, Zheng et al. [20] achieved a structural feature size of 10 μm in the production of metamaterial lattice structures. In 2015, a novel approach was introduced by Tumbleston et al. [21], which involved using an 'oxygen-containing dead zone' to ensure that uncured prepolymer is constantly available at the fabrication window and the printed part. This technique represented a significant advancement in the field, as it allowed for faster printing of complex geometries CLIP technology has a printing speed that exceeds 300 mm/hour, allowing parts to be produced in minutes rather than hours. In the z-direction, the printing speed can reach up to 1000 mm/h [22].

Researchers have been striving to improve printing speed, increase print area, and enhance surface quality in AM in recent years. However, traditional layer-by-layer printing regimes in DLP have limited the printing modalities. In 2017, Shusteff et al. [23] introduced a novel approach to holographic printing, allowing for the production of complex 3D structures. The method used three orthogonally directed light beams intersecting and superimposed to offset the limited axial resolution from other beam directions. Despite the progress in printing efficiency, material contamination during multi-material printing processes remains a significant challenge in DLP technology. Kowsari et al. [24] proposed an innovative method for removing residual liquid resin from cured 3D substrates using an air jet 58% faster than existing methods. Meanwhile, Amir et al. [25] demonstrated the possibility of multi-materials with microfluidic chip technology by printing a rat vasculature network. In 2019, Hayden Taylor's group introduced computed axial lithography (CAL), a volumetric AM method that generates various geometrical exposures from multiple angles, achieving volumetric photopolymerisation [26]. Furthermore, CAL was utilised to print trabecular bone models, highlighting the ability of 3D bioprinting by CAL [27]. Walker et al. [28] proposed a new 3D printing method called high-area rapid printing (HARP), which utilises a mobile liquid interface to minimise adhesive forces between the interface and the printed object, thus allowing for high-speed printing. In 2022, Kang et al. [29] designed a digital photolithography system with a 180 nm feature size based on a DMD and a 1:200 scale projection objective. As DLP technology continues to be utilised in diverse fields, many advancements have been made, showcasing its potential for high precision and fast printing processes. Moving forward, the focus is shifting from high precision to achieving fast multi-material printing

Figure 2. Historical evolution of DLP technology.

capabilities, thereby expanding the possibilities of DLP technology.

3 The DLP technology

3.1 Principle of DLP printing

DLP technology utilises a layer-by-layer process to fabricate intricate 3D structures. To create 3D models, specialised 3D modelling software is employed, which generates STL files that are subsequently sent to the slicing software. As shown in Figure 3(a), dynamic bitmap images are generated by the DMD chip and projected onto photosensitive resins using UV light. The photosensitive resin of the resin vat takes the shape of each layer's mask pattern through a projection lens optical system, and the UV light triggers photopolymerisation, converting the liquid-state polymer into a solid-state. The printing build platform moves in the Z-axis direction driven by the motorised stage after each layer's photopolymerisation is complete. New images induce further photopolymerisation until the 3D structure is fully printed (Figure 3b). Figures 3(c) and (d) illustrate the micro coil array and micro matrix structure employed in the DLP technique.

DLP typically uses two main geometric configurations: 'Top-Down' (Figure 4a) and 'Bottom-Up' (Figure 4b). In the 'Top-Down' projection, solidification occurs at the bottom of the vat, while in the 'Bottom-Up' projection, it occurs at the air-liquid interface. The 'Top-Down' configuration can mitigate the effects of gravity on the cured structures but may cause convex undulations due to surface tension. The recoating blade is crucial

for uniform resin distribution, especially for large cross-section layers (Figure 4c), but may decrease cell biological activity, making it unsuitable for 3D bioprinting [32–34]. Additionally, the 'Top-Down' approach results in a smoother surface of the cured structure (Figure 4d), but the fracture path is more random and can cross over from one layer to the following (Figure 4e). Compared to the Top-Down, the 'Bottom-Up' approach offers a more compact system but presents challenges in separating the photopolymerised structures from the substrate. Researchers typically use a vat-tilting mechanism or oxygen-permeable membranes to reduce the separation force. The vat is commonly coated with PDMS or Polytetrafluoroethylene (PTFE) to enhance release properties (Figure 4f) [35]. With the 'Bottom-Up' approach, slices that makeup objects are well-defined, resulting in a staircase-like effect (Figure 4g). The fracture path is relatively flat and mainly occurs at the interface between adjacent slices (Figure 4h).

For high-precision 3D printing, post-processing is crucial for enhancing mechanical strength, such as Young's modulus and ultimate tensile strength (UTS) [36]. Agitation and ultrasound are two ordinary methods for cleaning uncured photopolymer [37]. Residual resin on the cured surface can result in defects that affect the cured structures' stability, surface integrity and functionality. Therefore, compressed air is used to dry the cured structures to eliminate any remaining solvents or uncured photopolymers. However, it should be noted that if the cured part is post-cured for an extended period, some mechanical properties like UTS will decrease, resulting in the cured
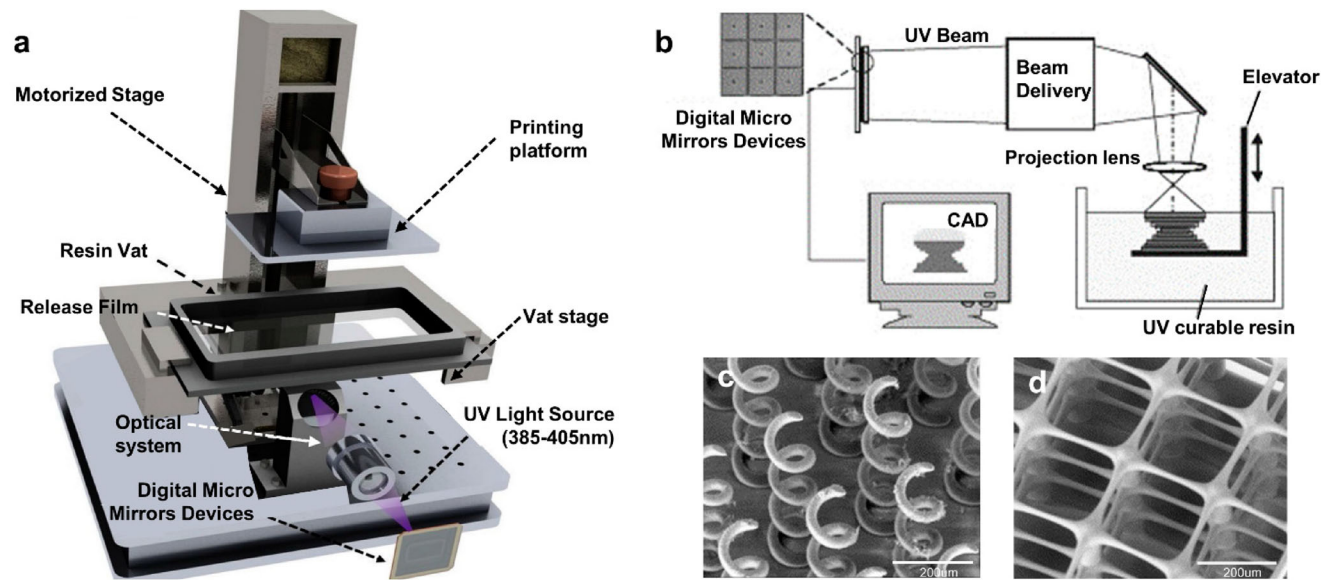
Figure 3. (a) Schematic representation of a DLP printing system. Reproduced from [30], reproduced with permission from [31]. (b) The high-resolution DLP printing system. (c) Micro coil array with a coil diameter of 100 μm. Scale bar: 200 μm, (d) Micro matrix. Scale bar: 200 μm. Reproduced with permission from [14].
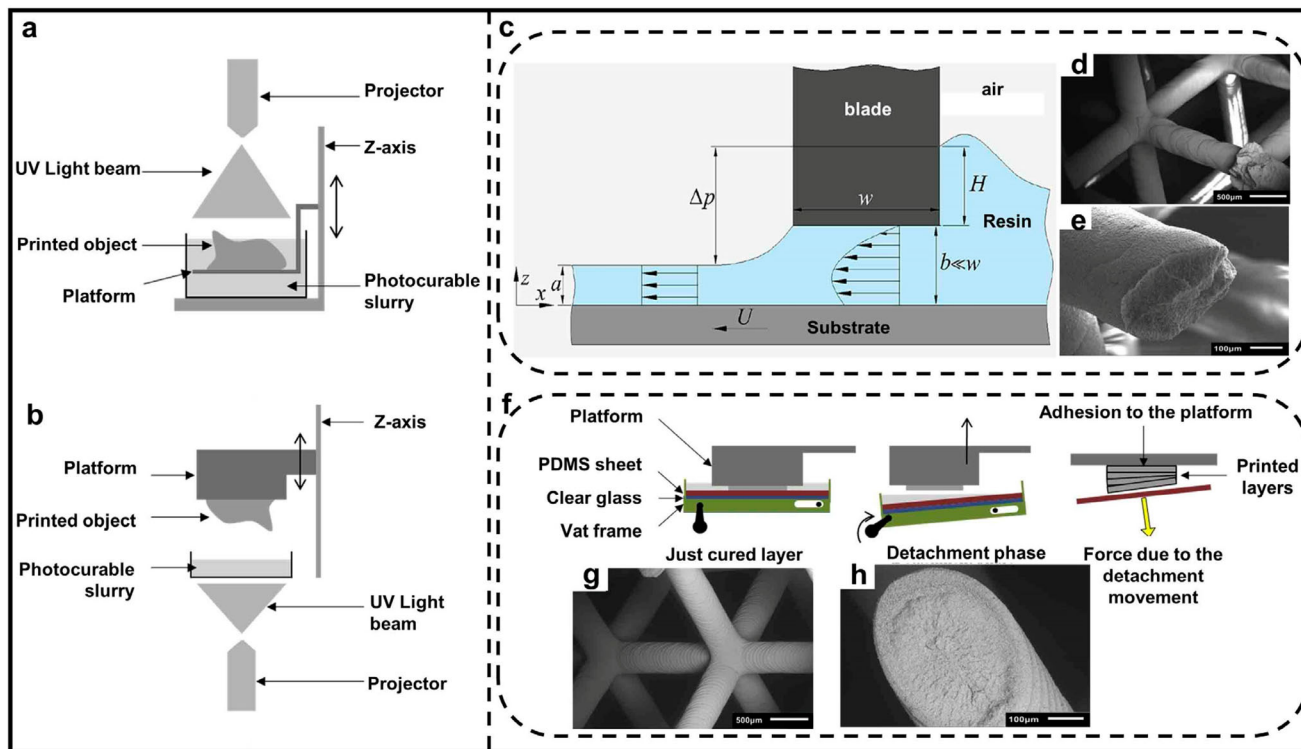
Figure 4. (a) Schematic of the 'Top to Down' DLP printing, (b) schematic of the 'Bottom to Up' DLP printing. Reproduced with permission from [34], (c) the blade of 'Top to Down' DLP printing, reproduced with permission from [33], (d–e) the structures fracture surface of 'Top to Down' DLP printing, (f) schematic illustration of detachment movement in 'Bottom to Up' DLP printing, (g–h) the structure fracture surface of 'Bottom to Up' DLP printing Reproduced with permission from [34].

part becoming more brittle [38]. Thus determining the appropriate post-curing time is critical for photopolymerised structures.

3.2 Hardware system of DLP

The DLP printing system comprises four subsystems (Figure 5): the DLP light engine, projection lens, motorised stage and resin vat. The DLP light engine comprises UV light, DMD and associated optics. This discussion will now concentrate on the subsystems of the DLP printing system.

DLP light engines: DLP light engines typically operate in the UV spectrum of 385 to 405 nm, which is highly efficient for photopolymerisation. The complex lens assemblies of DLP light engines collect and redirect scattered UV rays into a parallel beam to optimise the wide divergence angles emitted by UV light output [39]. The dynamic mask, the centrepiece of DLP light engines, includes a liquid crystal display (LCD) or a

DMD [40]. Although the LCD was the first dynamic mask used in 1997, the light absorption is considerably increased during the ON mode, and its switching speed of around 20 ms substantially hampers its use [9, 14, 41, 42]. On the other hand, DMD offers superior contrast to LCD and is better suited to handle UV light. This is why almost all high-precision DLP printing systems on the market today are using DMD. DMD is a binary device that can only generate two grayscale values, ranging from pure white to pure black (Figure 6b). The single micro-mirror in Figure 6(c–e) can be changed through the tensile strain of the hinge by adjusting the bonding positions of the nanowire clamped on the micromirrors to generate different patterns. Pyo et al. [43] developed a custom-designed 3D printing system using DMD technology. The system leverages the unique working principle of DMD to create user-defined gradient stiffness and microstructures with smooth, complex surfaces in seconds (Figure 6a).
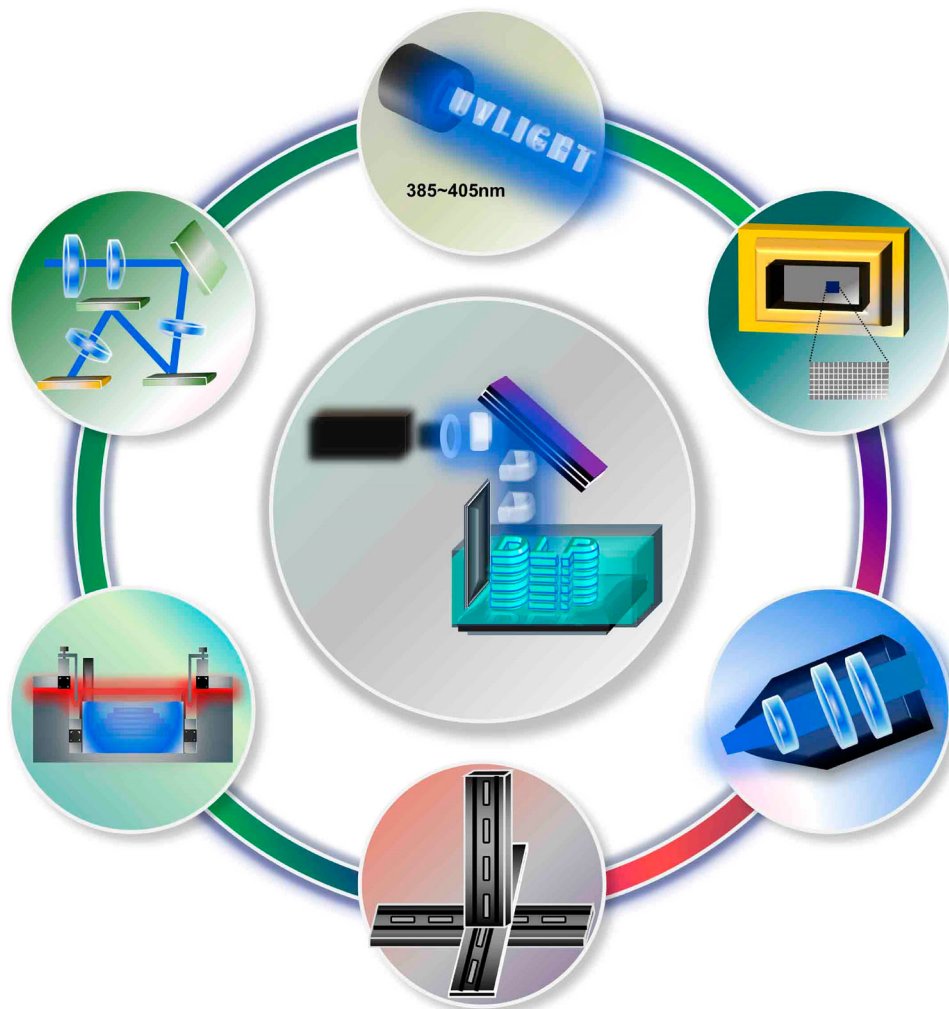
Figure 5. The schematic of fundamental components of DLP systems.

Projection lens: The projection lens plays a vital role in magnifying or reducing the 2D image displayed by the DMD to the projection plane while ensuring light uniformity. DLP light engines usually have two projection lens configurations: telecentric and conventional non-telecentric. Low, lightweight DLP systems are known for their non-telecentric design, as shown in Figure 6(f) [45]. In optical systems, the telecentric lens plays a crucial role in ensuring the projected image has constant magnification over the field of view. As depicted in Figure 6(g), one of the critical features of telecentric lenses is the use of total internal reflection (TIR) prisms, which are positioned between the projection lens and the DMD to eliminate image distortion. The TIR angle also reflects backscattered light that does not follow the parallelism, thereby increasing uniformity efficiency at the expense of reducing contrast [46, 48]. Furthermore, the magnification or image size of the telecentric lens does not change with focus, and this assembly method minimises the space between the optical components and the DMD, making it a popular choice for DLP light engine design.

Motorised stage: Motorised stages ensure the precision and surface quality of 3D-printed objects. A motorised stage consists of several critical parameters, including 'Minimum Incremental Motion', 'Accuracy', 'Bi-directional Repeatability Accuracy' and 'Load Capacity', which are crucial to meeting the requirements of the DLP system. The 'Minimum Incremental Motion' is a theoretical value that may not directly correlate to the value used in the printing process. The 'Bi-directional Repeatability Accuracy' is the most critical parameter influencing the printing layer thickness, particularly for achieving smaller layer thicknesses. Despite the high resolution of DLP printing systems, they still have fabrication constraints [49], such as the layer stair-stepping effect that leads to poor surface finish. To address this issue, reducing layer thickness is a dominant approach in AM [50]. 'Load Capacity' is also a significant factor for DLP printing systems; having enough load capacity is essential for the smooth operation of the printing process, a prerequisite for achieving printing accuracy. This is because the motorised stage needs to carry the cured structures upward or downward to achieve the thickness of a single layer. This process continues until the 3D structures are fully printed [51].

Resin Vat: In DLP-based 3D printing, the resin vat is the receptacle that holds the photopolymer. The 'Bottom-Up' DLP printing system has a transparent window in the resin vat, allowing UV light to pass through from underneath the DLP light engine. In this system, the layers attach between the cured and glass windows. To reduce the adhesion forces, researchers often coat the glass with PDMS or PTFE [52]. An oxygen-permeable membrane is also an essential component of the resin vat, necessary for measuring separation forces with different membranes. Pan et al. [53] reported a separation force of 20 N when creating a 625 mm^2 area using a PDMS coating. Liravi et al. [47] proposed a force separation model to investigate the peeling effect of PDMS film after characterising the cured separation force. The separation process could be divided into four parts (Figure 6h), which are time-consuming and may cause damage to the cured surface. Wu et al. [54] reported that using PDMS coating might potentially compromise the structural integrity of the 3D-printed structures and degrade more rapidly than PTFE membranes. The PDMS coating may also create an opaque surface that scatters light, adversely affecting printing accuracy and resolution. Kunwar et al. [35] tested the PDMS film and Teflon film, and they found that a 600μm PDMS film could generate a similar non-adhesive zone to a 45 μm Teflon film (Figure 6i), which is an important area that defends the photopolymerisation process and reduces the adhesion force. In the 'Top-Down' DLP printing system, a release film with hydrophobic properties is used to ensure that the original build surface is level and to reduce the adhesion of the cured structure to the film, thereby ensuring that the cured structure adheres successfully to the print plate. The design of release film clamps is essential for resin vats. The self-peeling vat concept was proposed in 2019 by Ribo et al. [55]. Various vat designs have been optimised to facilitate easier membrane replacement, incorporating features such as even screw distribution, hole perforation, and a bracket mechanism, as well as offsetting the glass window from the centre to create a different peeling angle, which reduces adhesive forces and enables a self-peeling method of detachment [56].

3.3 Theoretical model for the DLP photopolymerisation process

In 1992, Jacobs introduced the initial and fundamental model that describes the curing depth of a laser beam when scanning along a straight line [57]. In 3D printing using photopolymerisation, each layer is exposed to a single, total irradiation exposure. The energy of irradiation (**E**) delivered to the resin surface can be expressed mathematically as an Equation (1). [58]. In the 'Working curve model' model, the optical irradiance at the resin surface at $z = 0$ is represented by I_0 and t represents the light intensity and exposure time. E_{max} is the maximum energy, which corresponds to the energy density of a light beam before it enters a
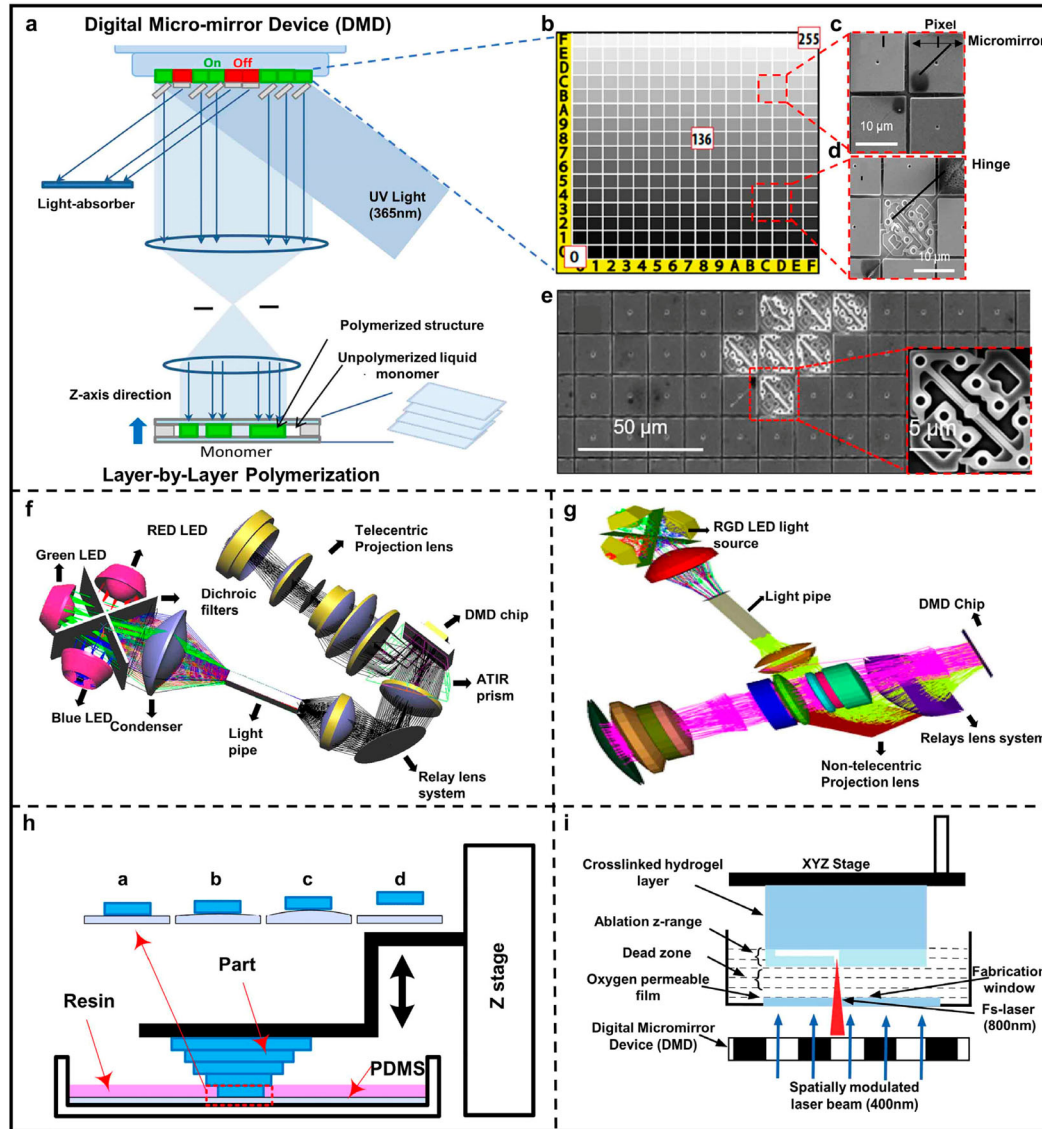
Figure 6. (a) The working mechanism of DMD-based on DLP, reproduced with permission from [43]. (b) The grayscale colour representation of a DMD using hexadecimal values (0–255). (c) Micromirrors of DMD. Scale bar: 10 μm. (d) The inner hinge of the DMD Scale bar: 10 μm. (e) The torsion hinge and electrodes of micromirror arrays on the DMD chip, reproduced by permission from [44]. (f) Schematic of a telecentric projection lens for digital light engines [45]. (g) Schematic of a non-telecentric projection lens for digital light engines [46]. (h) Illustration of the separation mechanism of DLP (button to up), reprinted with permission from [47]. (i) A schematic illustrating the resin vat assembly and critical parameters, such as the dead zone, for the DLP-based 3D printing system(button to up), reprinted with permission from [35].

pool of photopolymer resin. The 'Working curve model' proposed by Jacobs can be expressed in Equation (2):

$$E = tI_0 \tag{1}$$

$$C_d = D_p I_n\left(\frac{E_{max}}{E_c}\right) \tag{2}$$

Herein, the variable C_d represents the depth or thickness of the cured resin layer. The principle proposed by Jacobs introduces two essential parameters: the curing time penetration depth D_p and the energy required for polymerisation E_c [31]. The penetration of light obeys a Beer–Lambert law [59, 60], D_p is a function of the absorbance characteristics and composition of the polymer system [61], which is the depth at which the light intensity is reduced to $1/e$ of its initial value due to absorption by the photopolymer resin. E_c is the exposure dose at the 'gelation point' where a rapid increase in viscosity is observed, and the photopolymer resin no longer flows freely [57]. D_p and E_c are the only two parameters that rely purely on the photopolymerisation process [62], and optimising the process parameters involves determining the suitable values for D_p and E_c. Moreover, upon examination of Figure 7(a), it evident that D_p is the slope of the 'working curve', which is obtained from the actual measurement data on print layer thickness versus exposure time (energy). The energy E_c or exposure time T is the intersection of the straight line of the side measurement data with the X-axis.

However, the theoretical calculation of the 'cured structure thickness' C_d for different photosensitive resins varies. There are generally two scenarios: photosensitive resins mainly consist of monomers and photo-initiators or monomers, photo-initiators and photo-absorber. In the first case, the penetration depth D_p and the whole solidified thickness C_d could be represented [57] as

$$D_p = \frac{1}{2.3\varepsilon[PI]} \tag{3}$$

$$C_d = \frac{2}{2.303\varepsilon[PI]} I_n\left(\frac{E\sqrt{[PI]}}{\alpha_1 \beta}\right) \tag{4}$$

Lee et al. [61] considered the photo-polymerisation kinetics to develop a prediction model. Importantly, they demonstrated that the maximum value of C_d, denoted as ($C_{d,max}$), which is the optimal energy dose required for maximum cross-linking efficiency. Lee's model is an important contribution to predicting the maximum thickness of the 'gelation point', which is the minimum cured thickness attainable with DLP processing. This model involves two constants, namely α_1, which describes the chemical system (including kinetic

constants) and relates to photo-polymerisation processing conditions, the constant of the chemical system (comprising kinetic constants), and β is the constant of photo-polymerisation processing conditions [64].

$$C_{d,max} = \frac{E^2}{6.259\varepsilon\alpha_1^2\beta^2} \tag{5}$$

Controlling UV light penetration and getting a minimum layer thickness is critical to eliminate the 'staircase effect' and achieve high-resolution structures in the vertical direction. Therefore, the DLP polymer systems sometimes require the incorporation of photoabsorbers. When photo-absorbers are incorporated into a polymer resin formulation, the effect of the absorber concentration [A] must also be considered. Modified equations (6 and 7) [65] are used to determine D_p and C_d, which take into account the influence of absorber concentration [A]. The relationship between the change of photo-initiator, photo-absorber concentration and curing layer thickness could be shown in equations (8 and 9). The relationship is described by the molar extinction coefficients of the photo-initiator and the absorber, denoted as ε_{PI} and ε_A, respectively. An analysis of this relationship reveals that the cured thickness will increase with the concentration of the photo-initiator but decrease with the increasing concentration of the photo-absorber.

$$D_p = \frac{1}{2.3(\varepsilon_{PI}[PI] + \varepsilon_A[A])} \tag{6}$$

$$C_d = \frac{I_n\left(\frac{E\sqrt{PI}}{\alpha\beta}\right)}{2.3(\varepsilon_{PI}[PI] + \varepsilon_A[A])} = \frac{I_n\left(\frac{E^2[PI]}{\alpha^2\beta^2}\right)}{2.303(\varepsilon_{PI}[PI] + \varepsilon_A[A])} \tag{7}$$

$$\frac{d[PI]}{dC_d} = \frac{\varepsilon_{PI}I_n\frac{e\alpha^2\beta^2}{E^2[PI]} + \varepsilon_A[A]}{2.303[PI](\varepsilon_{PI}[PI] + \varepsilon_A[A])^2} \tag{8}$$

$$\frac{d[A]}{dC_d} = \frac{\varepsilon_A I_n\frac{E^2[PI]}{\alpha^2\beta^2}}{2.303(\varepsilon_{PI}[PI] + \varepsilon_A[A])^2} \tag{9}$$

$$L_w = \omega_0\sqrt{2\frac{C_d}{D_p}} \tag{10}$$

In addition to the thickness of the cured layer, the width of the 3D structure after curing is also an important consideration. The cured width, denoted as L_w in Jacob's model is shown in Equation (10). This effect is particularly applicable to 'Top-Down' configurations, where crosslinking primarily occurs on the top surface of the resin (Figure 7b). The width of the curing surface is directly proportional to the radius of the UV
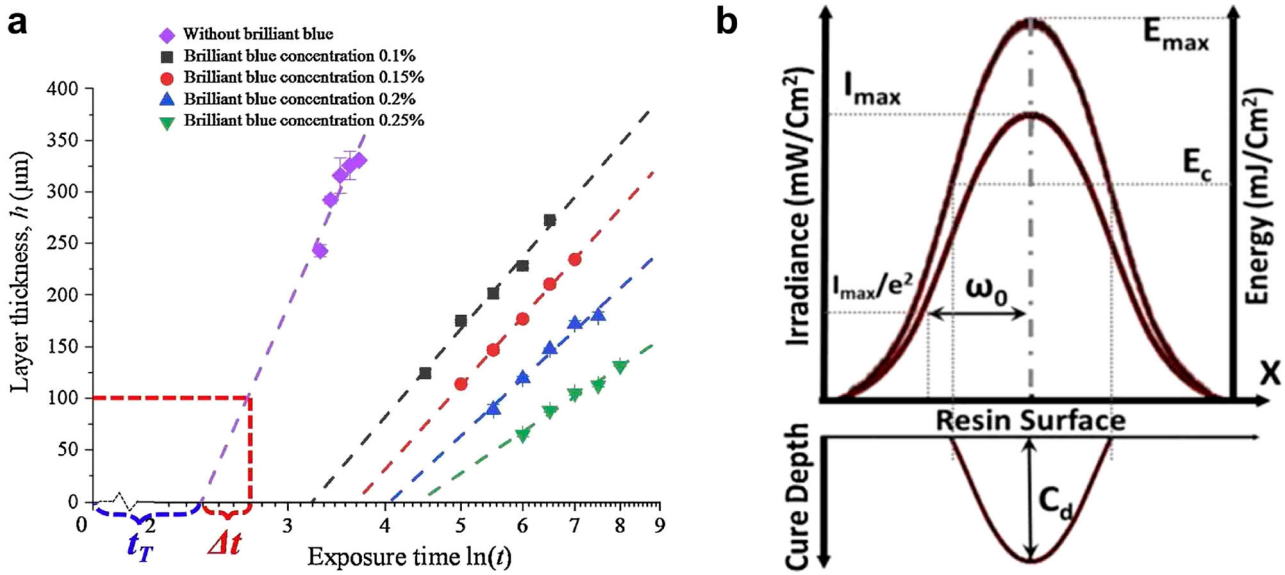
Figure 7. (a) The experimental data of the layer thickness h with exposure time t (the dashed lines are the linear fitting of the experimental data), reproduced with permission from [31]. (b) The distribution of irradiance exposure and cure depth of a UV beam, reproduced with permission from [63].

light beam (ω_0) at the top resin surface. The cure width is also proportional to the square root of the ratio C_d/D_p. Therefore, the cured width increases with higher cure depths C_d; however, it does not increase linearly with the penetration depth D_p. The width of the curing surface is strongly dependent on the diameter of the polymer chains D_p, particularly when there is a change in the resin composition. Recognising that photocuring accuracy is partly dependent on the material composition is essential to accurately control the depth of the cure and predict the width of the cure.

4 Commercial DLP equipment

DLP technology harbours the immense potential to function as a sophisticated precision polymer micro-manufacturing technology encompassing the entire value chain from concept development and fundamental theory establishment to equipment design, assembly, optimisation, and product fabrication. Over the past forty years, many superior quality DLP 3D printers have surfaced. The commercial DLP printer market can be bifurcated into industrial DLP 3D printers and desktop DLP 3D printers. An analysis of the data showcased in Figure 8 indicates that the essential specifications of industrial DLP 3D printers can be summarised as follows:

- Printing resolution: The resolution of commercial DLP 3D printers is a crucial parameter affecting printing quality. While some companies like 3D Systems, Nextdent and EnvisionTEC have established themselves as

leaders in dentistry, jewellery and hearing aid applications, their focus in these specific areas limits the achievable printing resolution is not higher. Additionally, the CeraFab System S230 (Lithoz) offers a resolution of 50 μm, and the ProMaker 'LD20' series with an XY resolution of 42 μm. These printing resolutions can represent the resolution of most printers on the market today. For 3D bioprinting, Engineering for Life (EFL) has achieved a resolution of 25 μm for soft polymers such as hydrogels. Meanwhile, for high-resolution DLP printing, Boston Micro Fabrication (BMF, China) and Nanofabrica (USA), both established in 2016, offer printers with the highest precision in the DLP market. The S140 series by BMF provides an impressive resolution of 2 μm. Nanofabrica's 'Fabrica 2.0' series delivers 1–5 μm layer thickness and an XY resolution of 1.9 μm, producing highly precise 3D parts with a final roughness as low as 0.8 μm.

- Printing speed: Achieving high printing efficiency in commercial 3D printers necessitates high printing speeds. The printing speed of conventional commercial DLP printers primarily relies on the movement speed of the Z-axis motorised stage. The fastest print speed of traditional DLP companies such as Phrozen, Creations (American), and 3D Systems is mainly concentrated from 30 to 100 mm/h. Notably, Gizmo3D (Australia) has developed a printer showcasing exceptional printing speed, producing objects with dimensions of $150 \times 80 \times 26$ mm^3 in a mere six minutes. In [66], Carbon introduced a 3D printing technology called 'Continuous Liquid Interface
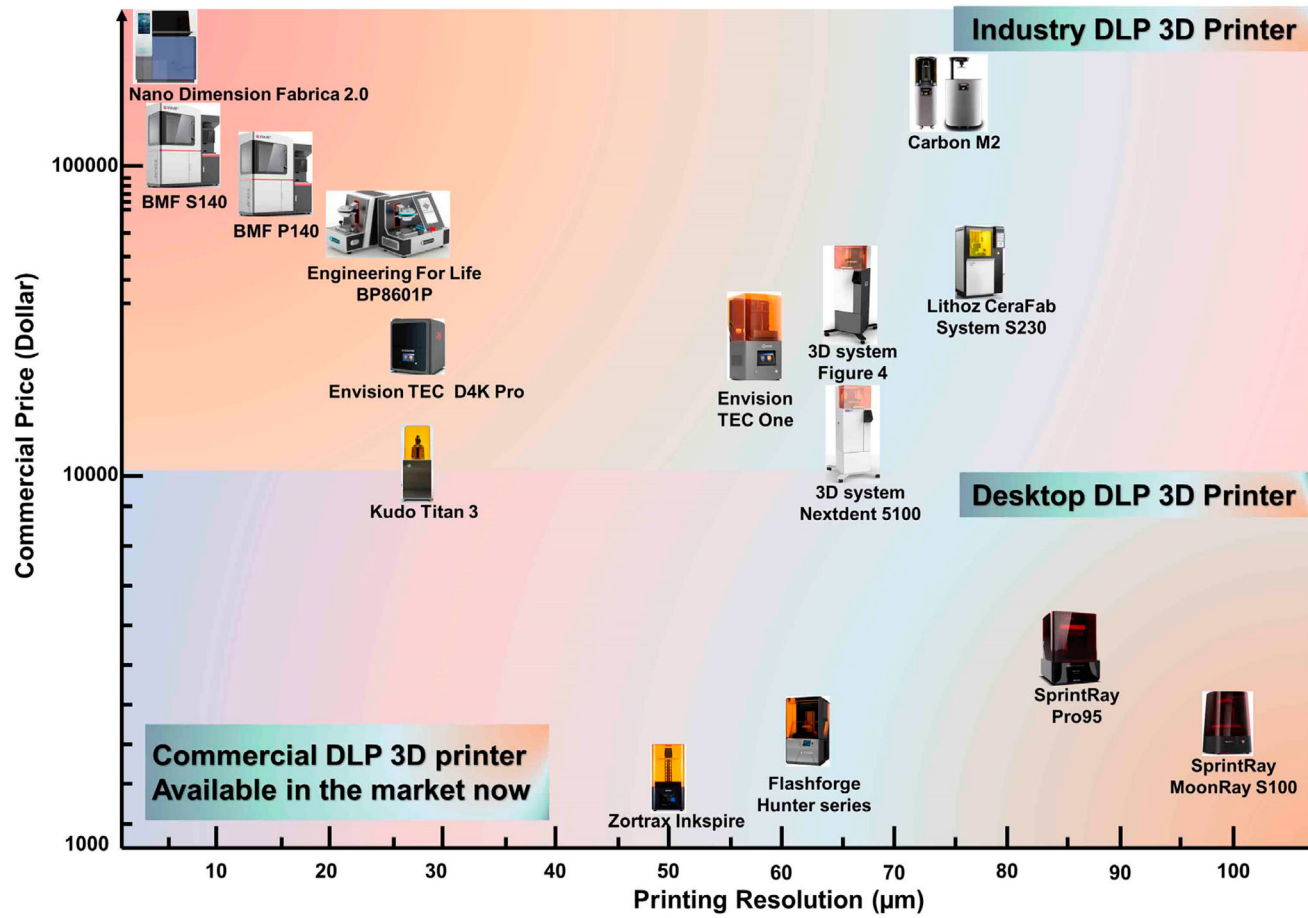
Figure 8. Selected some commercially available DLP 3D printers currently offered in the market, indicating commercial prices and printing resolution achieved

Production' (CLIP). This revolutionary technology enables significantly faster printing speeds than commercial DLP 3D printers, with a speed improvement ranging from 25 to 100 times (1000 mm h^{-1} in the z-direction). Consequently, Carbon's 3D printers are currently the fastest DLP printers available.

- Printing area: The print area of commercial DLP 3D printers is usually a few tens to a few hundred cubic millimetres. The relationship between printing resolution and printing area is often characterised by a delicate balance, wherein directly enlarging the printing area will reduce printing accuracy. Nevertheless, attaining a large-scale printing area is important across various application scenarios. Consequently, achieving an optimal equilibrium between printing accuracy and printing area has become a critical consideration within the commercial market. To address this challenge, EnvisionTEC has introduced the 'EnvisionTEC one', which offers an expansive printing area measuring $450 \times 371 \times 399$ mm^3 with compromised printing accuracy (100 μm). The newest printer from BMF, the S230 series, achieves 2 μm print accuracy and an increased print area of $1720 \times 750 \times 1820$ mm^3 through stitching technology and a series of compensation algorithms; it truly realises high-precision, large-area printing.

Although the market for commercial DLP 3D printers is significant, several challenges remain to be addressed. First, the printing resolution of industrial DLP 3D printers refers to their voxel resolution or X-Y resolution rather than the minimum achievable print feature size. Due to hardware, software, and polymer system constraints, the printing accuracy is often far from the theoretical printing resolution. Additionally, many commercial printers are proprietary and do not allow for open-source development, limiting application development by researchers. Academic research often leads to novel technological breakthroughs, and numerous successful companies have originated from universities. For instance, Carbon 3D and the University of North Carolina reported a revolutionary improvement in micro and nano 3D printing technology, Continuous Liquid Interface Manufacturing (CLIP), in Science in 2015 [22]. With the aid of CLIP technology, Carbon currently has customers in 17 countries and continues to expand globally [66]. Therefore, the development of DLP technology encompasses not only commercial development and applications but also the continuous pursuit of technological advancements and innovative applications in academia.

5 The materials used in DLP

5.1 Free-radical polymerisation

Polymerisation is a chemical reaction that combines small monomer molecules to form a polymer. There are two basic types of polymerisation: step polymerisation and chain polymerisation [67]. In chain polymerisation, the chemical reaction needs to be initiated by catalysts such as free-radical initiators, cationic and anionic initiators [68]. Therefore, chain-growth polymerisation consists of free-radical polymerisation, anionic, cationic and coordination polymerisation [69]. Free radical chain polymerisation is the most commonly used in commercial synthetic polymers, and it involves a chain reaction where free radicals initiate and propagate the polymerisation process [70]. The free radical chain polymerisation can be activated by light, voltage, chemical redox triggers and mechanical force depending on how radicals are generated. Among these methods, photopolymerisation, where light is used to trigger free radical polymerisation, is widely used in many fields [71, 72]. Figure 9 illustrates the 'Free-radical photopolymerisation' process, encompassing radical generation, initiation, polymerisation and termination [57, 73, 74]. In the photo-polymerisation process, radical generation is initiated when free radicals R absorb energy (hv) from the photoinitiator (PI), leading to a chain reaction with a monomer (M). During the propagation step, each addition of a monomer (M) to the growing macroradical (M_n) with a chain length of n monomer units results in the formation of a larger macroradical ($M_{(n+1)}$). The principal reactions responsible for chain terminations include recombination, disproportionation, inhibition, and occlusion. In the 'Free-radical photopolymerisation' process, a series of interconnected steps takes place to ensure the successful polymerisation and curing of the material and termination reactions occur to finalise the curing process and stabilise the polymerised material.

5.2 Polymer system composition for DLP

Creating high-precision and high-resolution constructs through DLP printing necessitates the utilisation of highly efficient photo-initiators (PI) and UV photo-absorbers (PA) during the photo-polymerisation process. The photo-initiator stimulates the generation of reactive molecules, such as free radicals, accelerating the speed of monomer cross-linking. Meanwhile, the photo-absorber regulates the depth of UV light penetration during printing [58]. Notably, information on commercial
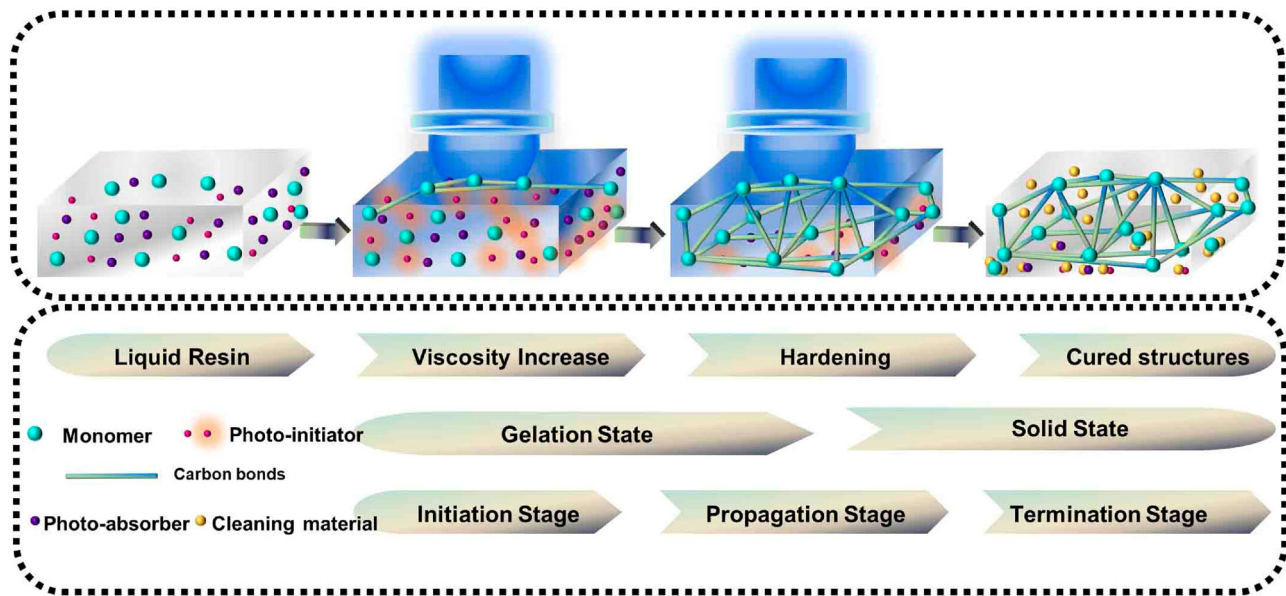
Figure 9. Free radical photopolymerisation of DLP polymer system

resins remains proprietary, with only a few studies mentioning the use of multifunctional (meth)acrylates in such materials [75]. Accordingly, developing a well-designed polymer system for DLP printing is crucial to ensure optimal performance. The attainment of high-precision printing necessitates a profound understanding of light-curing resins and the concomitant design of polymer resins.

5.2.1 Monomers

Monomers are small organic molecules with reactive functional groups that undergo polymerisation to form larger polymer chains. In photopolymerisation, monomers are designed for UV light-induced polymerisation, initiating chemical reactions that convert monomers into a polymer network. In DLP 3D printing, the fundamental constituents of the photopolymer system are monomers. The process involves the activation of reactive bonds in the monomers by UV light, which triggers polymerisation. As a result, long-chain polymers are formed at specific locations, ultimately resulting in the desired final structures. Monomers utilised in photopolymerisation frequently incorporate double bonds, exemplified by acrylates or methacrylates such as Poly (ethylene glycol) diacrylate (PEGDA), gelatin methacryloyl (GelMA) and methacrylate hyaluronic acid (MeHA). These double bonds display reactivity and readily engage in crosslinking reactions upon light exposure, establishing a three-dimensional polymer network. In addition, some functional particles or materials are mixed with monomers to produce functional polymer systems and print different functional 3D structures.

PEGDA is a modified form of PEG with acrylate groups, enabling photopolymerisation when combined with a photo-initiator. It fabricates micropatterned structures with feature sizes below 100 μm [76–78]. PEGDA also shows promise for drug delivery and tissue engineering applications [79–81]. GelMA is a gelatin-based hydrogel monomer derived from methacrylate modification [82, 83]. It is extensively used in tissue engineering, regenerative medicine, and drug delivery [84–94]. MeHA, a derivative of HA, is promising in CNS tissue engineering due to its association with the extracellular matrix [95]. It is also versatile in cartilage and bone-like tissue engineering [96, 97].

Different particles can modulate the structure and properties of polymers, enabling specific functionalised designs. Rossegger et al. [98]. incorporated Fe_3O_4 nanoparticles into monomers containing reactive thiol (–SH) and alkene (ene) functional groups, allowing the printing of flexible 3D structures controlled by a magnetic field. Cazin et al. [99] introduced Fe_3O_4 nanoparticles into a curable thiol-acrylate system, making the composites mendable and malleable using bond exchange reactions activated by elevated temperatures. Lantean et al. [100] successfully fabricated magnetically responsive gears using a strategic combination of Fe_3O_4 nanoparticles and monomers containing acrylate and polyurethane functional groups, and they demonstrated the ability to program specific motions in the gears. Fantino et al. [101] incorporated $AgNO_3$ into a PEGDA, resulting in complex 3D pieces with promising electrical properties. Gonzalez et al. [102] used CNTs in a photopolymer system with PEGDA and PEGMEMA monomers to print conductive 3D objects. Salas et al.

[103]synthesised MXenes nanocomposites using Ti3C2TZ as the nanofiller and bisphenol A dimethacrylate (BPA-dma, > 98%) as the monomer. Through the implementation of DLP printing technology, they were able to fabricate conductive 3D structures. Gastaldi et al. [104] investigated incorporating copper iodide clusters into an acrylic matrix, producing photoluminescent devices. The resulting devices efficiently guided irradiation and converted it from UV to visible light. Ceramic nanoparticles (e.g. silica, alumina, zirconia and hydroxyapatite) dispersed in monomer matrices can be decomposed via high-temperature heating after printing. Halloran demonstrated the DLP printing of complex-shaped alumina structures, including piezoelectric ceramics [105–107]. These studies showcase the potential of incorporating particles into photopolymer systems for the fabrication of functionalised 3D structures.

In addition to diverse particle incorporation, integrating various materials with monomers is another effective approach for achieving functionalised designs in polymer printing. Cazin et al. [99] utilised acrylates for radical-induced chain growth polymerisation at 405 nm and bi-functional epoxy monomers for cationic curing upon UV exposure at 365 nm and print structures with locally controlled mechanical properties. Similarly, covalent bonds and dynamic non-covalent interactions offer unique properties like adaptability, self-healing, and recyclability [108–110]. Li et al. [111] demonstrated the recyclability and shape memory properties of polyurethanes based on Diels-Alder reactions. Analogously, hydrogen bonding and metal-ligand coordination enable self-healing and stimulus-responsive properties [112–114]. Binyamin et al [115] utilise a dual-cure epoxy oligomer, BAEMA, with alkylated melamine to develop a novel epoxy-based photopolymer with high thermal stability. Bobrin et al. [116] investigated the nanoscale morphology and mechanical properties of monomer mixture using macromolecular chain transfer agents and found bicontinuous nanostructured materials exhibited enhanced mechanical properties. Patel et al. [117] developed highly stretchable elastomers for DLP-based 3D printing by varying the ratios of epoxy aliphatic acrylate (EAA) and aliphatic urethane diacrylate (AUD). Cafiso et al. [118] used trimethoxysilylpropyl methacrylate as a monomer to develop methacrylated carboxymethyl cellulose (mCMC) hydrogels with controlled swelling and pH-sensitive characteristics. Recently, Caprioli et al. [119] developed a self-healing photopolymer system using Poly (vinyl alcohol) (PVA), acrylic acid (AAc) and PEGDA, enabling room-temperature 3D printing of complex structures with the self-healing ability.

5.2.2 Photo-initiators

In DLP printing, the photo-initiator plays a crucial role in promoting the conversion of photolytic energy, which induces polymerisation for improved crosslinking and printing efficiency [65, 120]. Photo-initiators are molecular compounds that produce high-energy, active species, such as free radicals or cationic [121–125]. To be effective, a photo-initiator should possess a high molar extinction coefficient at the UV light source wavelength and produce active initiating species, like free radicals. The concentration of the photo-initiator has a significant impact on the crosslinking time of the polymer, so the crosslinking time generally ranges from a few seconds to a few minutes at specific wavelengths of UV light. With a specific wavelength of UV light, this time can range from seconds to minutes [25]. The photo-initiator can be classified as Norrish Type I or Type II [126]. Type I photo-initiators are molecules that can be cleaved into radical fragments upon exposure to UV light at a suitable wavelength [58, 127, 128]. Type II photo-initiators require a co-initiator and carbonyl compound to achieve an excited electron state. Compared to Type I, Type II photo-initiators have a slower reaction rate [129]. Water is the most convenient and readily available solvent for hydrogel fabrication in biomedical applications developing water-soluble photo-initiators is essential. Therefore, a summary is made based on the current common photo-initiators. Using water as a solvent for hydrogel manufacturing is a more convenient and readily available option in biomedical applications. Consequently, we have undertaken a concise compilation and categorisation of photo-initiators based on the solubility in water [130].

  1. **Water-soluble photo-initiator**

- **2-Hydroxy-4'-(2-hydroxyethyl)−2-methylpropiophenone** (Omnirad 2959)**:** In the field of aqueous photocurable systems, Omnirad 2959 is a well-known and frequently employed water-soluble photo-initiator due to its minimal toxicity and extensive use in the fabrication of biomaterials [131, 132]. Despite these benefits, Omnirad 2959 exhibits poor absorption at the wavelengths of DLP UV light (385–405 nm), leading to low polymerisation efficiency. Furthermore, the limited solubility of the compound in water (0.47 w/w) requires extensive agitation, heating, or the addition of organic solvents during dissolution, which can be laborious [133, 134]. Nevertheless, even at low concentrations of around 1%, Omnirad 2959 remains a popular choice for photo-initiators in many applications.

- **Lithium phenyl-2,4,6-trimethyl-benzoyl phosphinate (LAP):** LAP has garnered much attention in bioprinting due to its superior efficiency, rapid conversion kinetics and high efficiency under a high-energy light wavelength of around 400 nm [135]. Furthermore, LAP's broader absorption spectrum allows it to be excited by 405 nm visible light, which is less harmful to cells in the 3D bioprinting field. As a result, LAP has emerged as a preferred photo-initiator for bioprinting owing to its rapid and safe properties. However, LAP's cost is a significant constraint that limits its usage. LAPwidely used water-soluble photo-initiators that enable cross-linking within seconds due to their faster reaction rates and solubility in water. Fairbanks et al. experimented in 2009 using a PEGDA solution with LAP or Omnirad 2959. They found that LAP-induced gelation of photopolymer resins was about ten times faster than those containing Omnirad2959, as shown in Figure 10(a) [127, 136]. In 2013, Lin et al. [137] used LAP as a photo-initiator with PEGDA to print specific shapes and design architectural hydrogel scaffolds.
- **2′,4′,5′,7′-Tetrabromofluorescein (Eosin Y):** Eosin Y is a biocompatible photo-initiator commercially available in either water-soluble or ethanol-soluble forms. The ethanol-soluble type stains more quickly and produces a more vivid red colour than the water-soluble variety. Eosin Y is a visible light-activated photo-initiator that has found application in bioprinting. Kim et al. [138] The first cell-attachable UV light curing bio-ink was recently reported, incorporating GelMA and Eosin Y, printed using a commercial projector beam (Figure 10b). The excitation of Eosin Y occurs within the UV light spectrum at wavelengths ranging from 490 to 650 nm.
- **Diphenyl(2,4,6-trimethyl benzoyl) phosphine oxide (TPO-based nanoparticle):** TPO is a widely used commercial photo-initiator that can be transformed into water-dispersible nanoparticles through a multi-component approach. TPO is an effective photo-initiator with an extinction coefficient over 300 times greater than the best commercially available Omnirad 2959. In 2016, Pawar et al. [134] utilised TPO nanoparticles as photo-initiators to fabricate a hydrogel structure (Figure 10c). Although TPO has a maximum molar extinction coefficient below 400 nm, its absorption spectra cover the violet light region. This property enables TPO nanoparticles to be compatible with commercial DLP printers that utilise 405 nm UV light for curing purposes [75].
- **Riboflavin (RF):** RF is a commonly used type II photo-initiator in 3D printing. It generates initiating radicals or radical ions through electron transfer or hydrogen abstraction reactions [140]. RF, along with triethanolamine (TEOHA), is a co-initiator in printing double-network ionic hydrogels [141]. The RF-TEOHA system and multi-walled carbon nanotubes (MWCNTs) are employed in DLP 3D printing of acrylamide and other acrylic monomers at 405 nm [142].

Unlike aqueous polymerisation, non-aqueous systems offer a wide range of efficient photo-initiators. As a result, we will now provide a brief overview of some commonly used water-insoluble photo-initiators.

2. Water-insoluble photo-initiator

- **Omnirad series photo-initiators**: The Omnirad series of photo-initiators is widely recognised as one of the most extensively used commercials. Bis(2,4,6-trimethyl benzoyl) phenyl phosphine oxide (Omnirad 819), renowned for its superior performance in curing at low concentrations upon exposure to sufficient amounts of UV radiation, is a remarkable example. 1-Hydroxy-cyclohexyl-phenyl-ketone (Omnirad 184), a highly efficient photo-initiator, is commonly used for initiating photo-polymerisation in chemically unsaturated prepolymers. These photo-initiators are readily soluble in conventional solvents such as acetone and toluene. Another photo-initiate 2-Benzyl-2-dimethylamino-1-(4-morpholinophenyl)-butanone-1 (Omnirad 369), which is well-suited for various applications, such as pigmented UV curable systems, photoresists, and printing plates. Recently, Fang and colleagues employed a straightforward yet versatile photo-initiator system consisting of Bis (eta.5-2,4-cylcopentadien-1-yl)-bis (2,6-difluoro-3-(1H-pyrrol-1-yl)-phenyl) titanium (Omnirad 784 (type I)) and camphor quinone (CQ)-ethyl 4-dimethylamino benzoate (EDAB) (type II) to print intricate architectures (Figure 10d) [139].
- **Diphenyl(2,4,6-trimethyl benzoyl) phosphine oxide (TPO)**: TPO has been identified as one of the most efficient photo-initiators for inducing free radical polymerisation of various monomers. TPO contains an 'aroylphosphinoyl chromophore', demonstrating a distinct absorption range of 350 to 380 nm, extending to 420 to 440 nm, with high molar extinction coefficients. TPO also exhibits excellent thermal and shelf stability and photobleaching properties. It is worth noting that the absorption spectra of TPO show favourable characteristics for cell encapsulation; this finding suggests the potential of TPO as a suitable photo-initiator for tissue engineering [143].

Numerous advanced photo-initiators have demonstrated remarkable performance; however, several
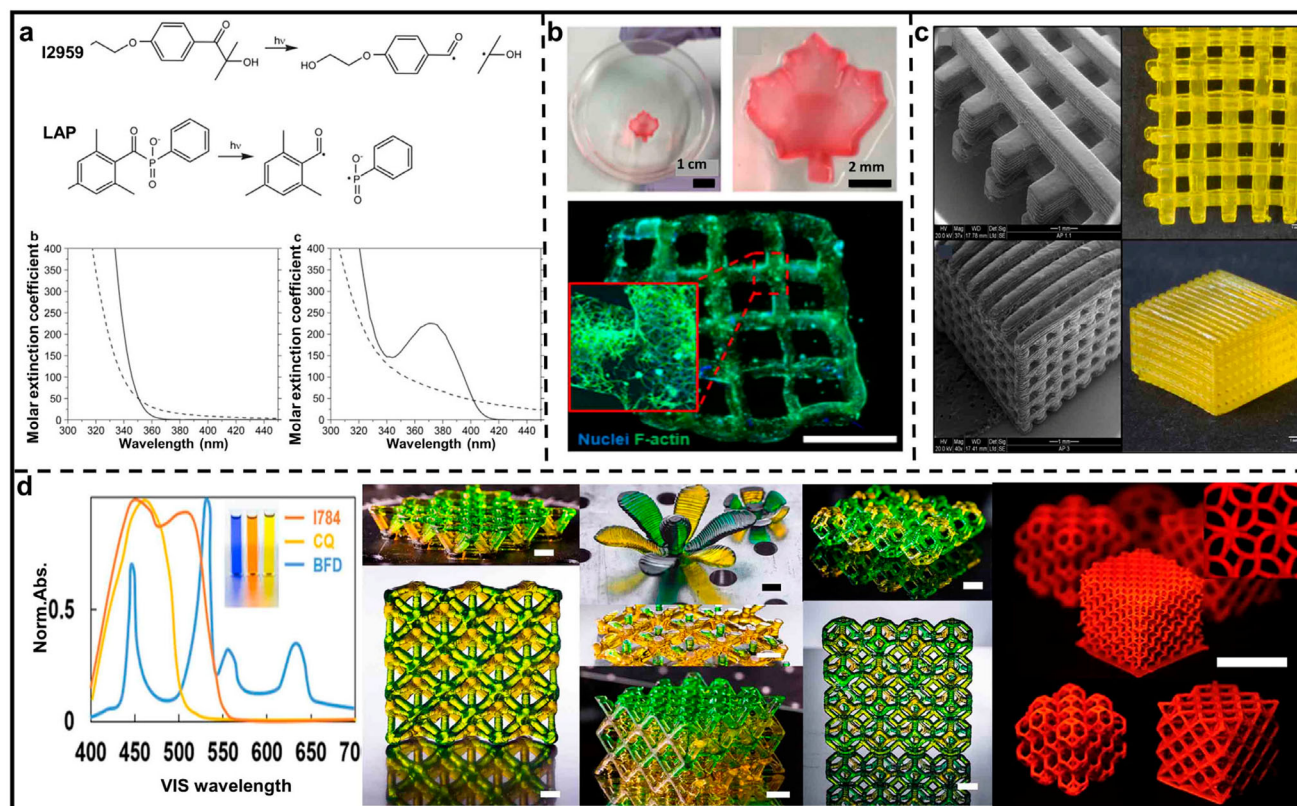
Figure 10. Summary of some common photo-initiators. (a) Cleavage of Omnirad2959 and LAP into substituent radicals following photon absorption, with molar absorptivities and cleavage products (dashed line) of the Omnirad2959 (left) and LAP (right), respectively They were reprinted with permission from [127]. (b) Maple leaf structure printed by Eosin Y-based photopolymerisation of GelMA bio-ink and NIH-3T3 cell-laden printed sample at day five stained with DAPI for nuclei (blue) and phalloidin 488 for F-actin (green) Reprinted by permission from [138]. (c) The structure was obtained from a photopolymer system with TPO nanoparticles Reprinted with permission from [134]. (d) Normalised absorption of photo-initiators Omnirad784, CQ, and blue food dye and substrates 3D structure fabricated using a polymer containing PEGDA, Omnirad784 (left) and Rhodamine B (right). Reprinted with permission from [139].

challenges and opportunities persist in these initiators' molecular design and application promotion. First, while a UV light photo-initiator that enables rapid and precise 3D printing is no longer an issue, enhancing the solubility of initiators in a broader range of solvents at the lowest possible cost is currently a focal point of research. A systematic study of promising organic dyes (commercials and newly synthesised) that have not yet been used in 3D printing could be captivating. Second, while numerous photo-initiators have been developed for non-3D printing purposes, only a few have been utilised in DLP technology. In particular, biocompatible and biodegradable macro-photo-initiators for 3D printing are largely unexplored in bio-printing. Pursuing novel photo-initiators or photo-initiating systems represents a promising avenue for advancing the field of photopolymerisation 3D printing. The variety of natural photoactive compounds offers an excellent source for developing a new photo-initiator that might cover the entire visible spectrum. These compounds have already proven potential to enable light-based 3D printing in the visible spectral range. The new natural and natural-derived photo-initiator will be used in more and more DLP 3D printing [144].

5.2.3 Photo-absorber

In DLP printing, UV exposure times and light intensities need to be scientifically adjusted to ensure accurate curing depths in complex geometries. One crucial element in photopolymer systems is the photo-absorber, preventing excessive polymerisation due to light scattering and enhancing Z-axis resolution and pattern fidelity [145]. The photo-absorber significantly impacts the UV energy distribution on the imaging surface by reducing the light energy absorbed by the photo-initiator and weakening the intensity of UV light. Hence, careful regulation of the photo-absorber concentration is critical to achieving an appropriate depth of cure and increasing the crosslink density to attain high-precision printing.

- **Dyes:** Dyes are added to the polymer to improve the features of the objects, such as resolution or strength and not affect the polymerisation process itself [65]. Cure depth relies on light absorber concentration and molar extinction coefficient. Dyes spatially confine polymerisation, preventing over-curing in width and depth [146, 147]. Tartrazine has been explored as a yellow food dye for potential use in various biomedical applications. These properties enable sufficient elution and transparency of hydrogels after fabrication [148]. In a study by Grigoryan et al. [149] in 2019, a vasculature network was successfully printed using a photopolymer resin composed of PEGDA and tartrazine via continuous liquid interface production (CLIP) technology. Another photo-absorber that has shown promising results in achieving 200 μm feature sizes with PEGDA hydrogels is Reactive-Orange-16, which has an absorption peak at around 493nm and is water-soluble [150, 151].

- **1-phenyl azo-2-naphthol (Sudan I):** Sudan I is a commonly utilised photo-absorber in DLP printing [58, 152]. As a member of the Sudan dye group, a set of lipid-soluble solvent dyes, Sudan I is not highly water-soluble. Nonetheless, it can dissolve in different solvents, including DMSO, ethyl acetate, ethanol, ether, acetone and benzene.

- **Reactive Orange 16:** Reactive Orange 16 has been used to avoid the curing out of the irradiated area and to control the thickness of each layer [153]. Reactive Orange 16 is the photo-absorber used to prevent the leaking out of light from the desired illumination area. It allows controlling the thickness of each layer during the printing process [101].

- **2-Nitrophenyl Phenyl Sulfide (NPS)** NPS is a cost-effective and easily available photo-absorber that has been identified as a suitable candidate for DLP printing systems, particularly when compared to other commonly used and easily dissolvable photo-absorbers such as toluene, chloroform, and methanol [152]. In the 480–420 nm spectral range, NPS exhibits significantly greater absorbance than certain food dyes, including Brilliant Blue, which results in weaker UV light penetration and enables the printing of high-precision 3D structures via DLP technology.

5.2.4 Crosslinker

Crosslinker plays a critical role in photopolymerisation as it governs the efficiency of step-growth reactions and subsequently influences the mechanical properties of polymer systems [154]. Lee et al. [155] studied UV-curable resins with varying monomer (butyl acrylate) and crosslinker (diurethane dimethacrylate) ratios in DLP printing. Results show that increasing diurea dimethacrylate can increase crosslinking density and improve mechanical properties. Zhang et al. [156] developed a robust shape-memory polymer system using tert-butyl acrylate (tBA (linear chain builder)) and aliphatic urethane diacrylate (AUD (crosslinker)). They found The AUD crosslinker endows high deformability and fatigue resistance to the tBA – AUD shape-memory polymers (SMP) system. Borrello et al. [157] utilised 1,6-hexanediol diacrylate as a crosslinker, achieving a 50-fold change in elastic modulus by adjusting monomer and crosslinker ratios. When printed, these

formulations maintained mechanical integrity, dimensional accuracy, and high feature resolution.

5.2.5 Radical scavengers

Photosensitive polymers are inevitably exposed to natural light during storage, transportation and printing. Without a radical inhibitor, visible light easily triggers the initiator to produce free radicals. This will further lead to chain-growth photopolymerisation, resulting in the irreversible curing of photosensitive gel ink. To avoid this undesirable photocuring reaction, it is usually necessary to add some radical inhibitors, which are used to eliminate the possible residual free radicals, preventing the small molecules in the photopolymer system from cross-linking before 3D printing [158]. The radical inhibitor is a kind of substance which can completely stop the free radical polymerisation of alkenes monomers [159]. The radical inhibitor molecules react with free radicals to form non-free radical substances or less active free radicals that cannot be initiated a reaction, thus terminating polymerisation [160]. The selection of radical inhibitors mainly depends on several properties, including high anti-polymerisation efficiency, solubility in monomers and adaptability to monomers. Hydroquinone (HQ) is one of the most commonly used radical inhibitors in photosensitive resin products [161]. Tocopherol, triallyl phosphates and naringenin are other free-radical scavengers [162, 163]. Similarly, $NaNO_2$, as an aqueous phase radical scavenger, prevents secondary nucleation reactions initiated by free radicals by reacting with and neutralising them [164].

5.2.6 Oxygen inhibitors

Oxygen inhibition effects have been a significant factor in the DLP printing procedure. The inhibition effect of molecular oxygen in free-radical photopolymerisation reactions has always been a key issue [165, 166]. To overcome oxygen inhibition, one is increasing light intensity or photo-initiator concentration; another is containing easily abstractable hydrogen atoms such as amines or thiols [167, 168]. Besides, photochemical methods may also be used to consume dissolved oxygen before polymerisation, which is based on light-absorbing species that sensitise singlet oxygen from dissolved molecular oxygen. Once it is produced, singlet oxygen can react with a scavenger such as benzofuran derivatives to form hydroperoxides or endoperoxides; these compounds are subject to further decomposition upon irradiation, thereby removing the molecular oxygen from the system [169, 170]. The effect of Triphenylphosphine as an oxygen scavenger in the free-radical photopolymerisation of acrylates was clarified. They observed that the effect of oxygen inhibition decreases in the presence of Triphenylphosphine. Additionally, Ligon, Samuel Clark et al. [171] detailed a summary of the current strategies for oxygen inhabits in the photopolymerisation process.

5.3 The characteristics of the polymer system

The direct influence of the polymer system on printing resolution and the resulting function of cured structures underscore the critical importance of discovering suitable polymer systems to enable DLP printing of high-accuracy, high-fidelity constructs. Furthermore, the polymer system needs to satisfy diverse requirements for various applications, such as micro-structure manufacture, by exhibiting controllable mechanical and chemical properties. In addition, it should show good printability, such as being easy to print, having good fluidity, solidifying quickly, and maintaining its final structure after printing. Determining the optimal formulation is thus the first critical step towards DLP printing success.

· · **Printability:** Printability refers to the ability of the photopolymer to print 3D structures with high structural integrity [172]. The printability of a polymer system is a critical factor in printing high-fidelity 3D architectures, mainly regarding shape fidelity, cured structure, and mechanical stability [173]. Assessing the printability characteristics of photopolymers encompasses thoroughly examining their light-curing properties, adhesion, fluidity, etc. The light-curing characteristics of the photopolymers emerge as the fundamental and critical factors in evaluating their printability, with high sensitivity to the UV light source being essential for rapid and efficient curing upon exposure to UV light. The most used methods to evaluate the cure extent are differential scanning photo calorimetry (photo-DSC), real-time infrared spectroscopy (RT-IR), and confocal Raman microscopy [174]. Additionally, the adhesion of the photopolymers plays a foundational role in successful printing, especially in layer-by-layer DLP printing. Strong adhesion to previously cured layers is imperative for establishing a stable printing process and constructing reliable structures, effectively preventing inter-layer peeling and deformation, thereby ensuring overall print quality [175,176]. Similarly, the fluidity of photopolymers plays a pivotal role in the success of photocured materials. Fluidity directly influences the ability of photopolymers to flow smoothly during the printing process, and exceptional fluidity contributes to the production of detailed

and surface-flat structures [177–179]. Researchers utilise photopolymer to print specific design structures, followed by a comprehensive analysis of the printability characteristics of the printed structures to determine whether the photopolymer meets the print requirement. This systematic methodology fosters a thorough comprehension of the performance and behaviour of photopolymer throughout the printing process, ultimately enabling the identification and selection of the most optimal photopolymer for high-precision DLP printing applications. Thus the study of the printability of polymers is essential to achieve high-precision fabrication with DLP printing. Furthermore, in addition to designing printing strategies based on the properties of synthetic polymers, the printing process's in-depth study is necessary to determine the most suitable formulation and concentration of the resin components.

· · **Mechanical properties:** Mechanical properties are especially critical for most DLP applications, such as regenerating hard tissues and microfluidic devices, where appropriate mechanical strength is essential. Materials' mechanical properties are crucial in determining their suitability for a particular application. In contrast, materials with high mechanical strength and stiffness are more suitable for applications such as tissue engineering and microfluidic chips. The mechanical properties of photopolymer play a crucial role in printing, directly affecting the strength and durability of the printed structure. Firstly, tensile strength is a measure of the ability of the photopolymer to resist tensile forces, which is crucial to the overall strength of the printed part, especially when printing microfluidic channels, the photopolymer with high tensile strength can obtain a better channel structure, ensuring structural integrity and functionality [180, 181]. Secondly, flexural strength is the ability to assess the resistance of the photopolymer to bending forces, which is directly related to the bending performance and durability of the printed part. Particularly for curved shape structures, a higher bending strength ensures better printing accuracy and stability during use [182]. In addition, hardness is a measure of the ability of the photopolymer to resist localised compression or scratching [183]. A high hardness value means that the material is more resistant to abrasion and scratching, which is critical to the durability and longevity of the printed part, especially in applications where wear resistance is essential. Therefore, when selecting a suitable photopolymer, it is necessary to consider and evaluate these mechanical property indicators thoroughly. This ensures the appropriate photopolymer choice for specific applications based on different practical requirements.

6 Process parameters in DLP

The efficacy of DLP 3D printing is highly contingent upon the photosensitivity of photocurable material systems and the corresponding UV light illumination parameters, including UV light intensity and exposure time. Figure 11 provides an overview of the crucial process parameters involved. Notably, a more reactive photo-initiator and photo-absorber tend to yield stronger, high-fidelity constructs. Lower UV light intensity and shorter exposure times lead to reduced mechanical properties in 3D printed structures, compared to higher UV light intensity and longer exposure times. Additionally, the cured structures' final mechanical properties depend on the polymer's composition and concentration. Varying process parameters or polymer systems lead to different mechanical properties.

6.1 UV light exposure energy

The efficiency of photopolymerisation in DLP printing hinges significantly on the energy of UV light exposure, which is contingent upon both UV light intensity, exposure time, and wavelength for the DLP printing system [184]. UV light intensity and exposure time can directly impact gelation kinetics, rheological properties, mechanical performance, and degradation behaviour of cured structures. Based on experience, a lower UV light intensity with longer exposure time and suitable working distance is optimal for DLP printing. Post-curing combined with UV light exposure can be used to modify the mechanical properties of printed structures [185–187]. UV irradiation energy directly affects the crosslink density in UV-based photocuring. Upon UV exposure, photosensitive resins solidify through UV-induced chemical bond formation. Higher UV intensity promotes stronger interaction between photons and resin molecules, leading to increased energy absorption; this enhances the generation of free radicals and accelerates crosslinking, resulting in higher crosslink density. However, excessive crosslinking can cause unintended curing or occlusion of hollow structures, affecting printing accuracy. In addition, insufficient UV intensity leads to lower crosslink density, incomplete polymerisation and decreased mechanical properties. UV intensity and exposure time influence the intricate relationship between UV energy and crosslink density.
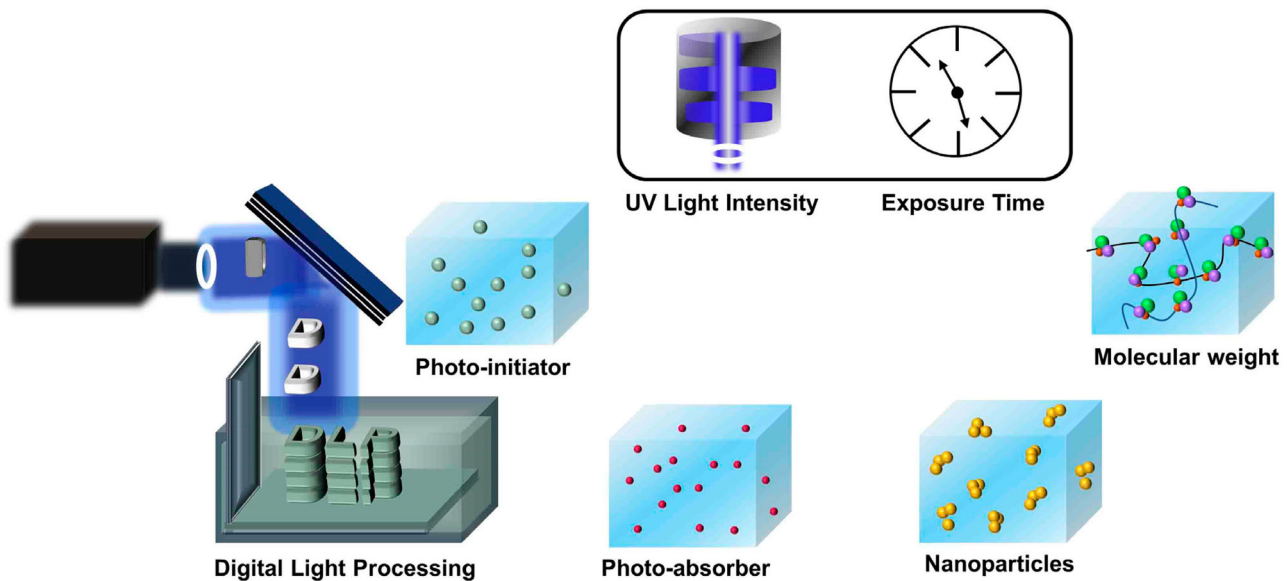
Figure 11. The process parameters of DLP.

Thus optimising these parameters is crucial for achieving the desired crosslinking density and material properties in UV-based 3D printing. Finally, the printing accuracy of micro-geometries is determined by print parameters such as UV light source wavelength, UV light intensity, exposure time and post-curing.

6.2 Resin system formulation

As previously mentioned, the photopolymerisation process in DLP printing primarily relies on one or more monomers, photo-initiators, photo-absorbers, etc., all of which contribute to printing efficiency, accuracy and mechanical properties. When considering a suitable photo-initiator for a DLP polymer system, it is crucial to consider the absorption spectrum and corresponding extinction coefficient to determine the overall free radical generation. The wavelength and absorption spectrum of the UV light source must be considered, as well as the degree of coincidence between the photo-initiator absorption spectrum and the UV light source [188]. The photo-absorber is another critical component of the polymer system that affects the absorbance of the polymer system, thereby influencing the vertical resolution of photopolymerised structures. Ensuring the curing depth remains within the optical depth of focus is crucial, as polymerisation can also occur in the out-of-focus plane, leading to decreased vertical resolution. Adding a photo-absorber to the polymer system can increase the polymer system's absorbance coefficient, allowing thinner layers to be printed. For example, the optimal photo-absorbers concentration for 3D printing of microfluidic devices with a

minimum layer thickness of 25 μm range from 0.2% to 0.3% [189]. Careful regulation of photo-absorbers concentration is necessary to ensure precise curing depth while preventing inadequate crosslinking density. Insufficient crosslinking density could result in a reduced crosslinking rate and density of the polymer system. Moreover, oxygen inhibition is a common issue generally found in free radical photocuring applications [190]. Oxygen can inhibit photopolymerisation by reacting with the reactive species generated during photopolymerisation. The presence of oxygen can slow down the rate of polymerisation. Adding oxygen inhibitors and increasing UV light intensity and initiator concentration are common methods to reduce oxygen inhibition.

In addition to the polymer components mentioned above, researchers have found that adding nanoparticles can improve printability, structure stability and mechanical properties. However, the uneven distribution of nanoparticles in the polymer system is a limitation when directly mixing these nanoparticles with a polymer system. To address this, some researchers have proposed nanoparticle polymer composite systems, such as the hydroxyapatite nanoparticles and PmLnDMA proposed by Yang et al. in 2020 [191]. This approach can enhance the inorganic-organic co-cross-linked nanocomposite network, improving the polymer system's mechanical performance. The molecular weight and concentration of the monomer also play a critical role in determining the mechanical and physical properties of the polymer system. Lower concentrations of polymers can decrease the stiffness and enlarge the pore size of the printed scaffold. At the same time,

higher molecular weight generally exhibits higher physical strength due to the less bendable bulk polymer network. The viscosity of the initial composition that increases as the polymerisation develops affects the kinetics from the start of the reaction, which mainly relies on the characteristics of the polymer system, such as molecular weight, chain length and intermolecular forces [192]. DLP printing systems require low-viscosity resins to ensure printing efficiency and avoid bubble formations, which may affect the integrity of the printed part. However, a too-low viscosity may hamper the mechanical properties of the printed structure. Therefore, viscosity and printing performance must be balanced to achieve an optimum DLP process. Indeed, an increase in viscosity of a low-viscosity system increases the reaction rate until an optimum viscosity (and hence the optimum reactivity) for a given system is obtained, but exceeding this viscosity leads to a reduction of the polymerisation rate and conversion due to early dominance of diffusion-limited propagation. For photopolymer systems of low- and high-viscosity monomers, the optimum viscosity was found to lie in the 3–5 Pa s [193].

The viscosity of light-curing resins significantly impacts the printing efficiency in DLP processes. Upon printing a layer of the structure, the printing platform moves up or down, and the new layer is automatically filled with resin before light curing commences. Ensuring precise horizontal alignment of the newly filled layer is paramount for achieving high print accuracy. However, when the photopolymer exhibits high viscosity during the auto-filling process, the return to a horizontal state may be delayed, consequently affecting the overall printing speed. To address the challenge of inefficient printing with high-viscosity photopolymer, some commercial printers have introduced 'scraper' to facilitate photopolymer flow. The scraper repeatedly moves back and forth across the photopolymer surface, reducing waiting time and ensuring an even distribution of the 'filled photopolymer'. Nonetheless, incorporating scrapers in certain 3D bio-printing applications may inadvertently damage delicate cells and disrupt specific processes, making them sometimes unsuitable as a fundamental solution for efficient high-viscosity printing. Conversely, in low-viscosity photopolymer systems, an increase in viscosity accelerates the reaction rate, thereby enhancing optimal reactivity; the optimum viscosity was found to lie in the 3–5 Pa s [193]. The viscosity increases encounters limitations in the light-curing reaction due to diffusion hindrance, impeding the propagation of polymer chains. Consequently, exceeding the threshold of the 'ideal viscosity' leads to decreased polymerisation rate and conversion.

Similarly, Careful consideration must be given to avoid excessively low viscosity, which may adversely affect the mechanical properties of the printed structure or cause structural collapse, thereby compromising overall printability. Achieving an optimal DLP process necessitates a delicate balance between viscosity and printability. Therefore, a comprehensive understanding of the interplay between viscosity and printability is indispensable in ensuring the success of DLP printing processes, particularly when striving for high-efficiency and high-precision results.

7 Precision microfabrication using DLP

DLP has been well used in printing microstructures and micro components with applications of biomedical engineering domains, microfluidic devices [194, 195], meta-surfaces [196] and metamaterials [20]. It is particularly useful as the fast-prototyping technology to fabricate microfluidic devices for making the device itself or master mould fabrication. Here we highlighted the progress of DLP 3D printing of microfluidic devices as a demonstration example of the high-precision requirements of DLP for microfabrication. Microfluidic devices have revolutionised the control and manipulation of small fluidic streams, enabling high-throughput capabilities and driving the miniaturisation of laboratory procedures [197, 198]. They have become indispensable in biology [199, 200] and chemistry [201], where precise manipulation and control of fluids in microliter quantities are paramount. A fundamental goal in microfluidics research is the development of lab-on-a-chip systems, which aims to condense traditional experimental and analytical instruments into miniature chip-based formats [202]. DLP technology has emerged as the leading choice for 3D printing in microfluidic mould production. Compared to traditional microfabrication techniques like lithography [203], wet/dry etching [20]. DLP printing offers significant advantages, including rapid printing, unparalleled accuracy, and superior surface finishes, and thus enhances the design flexibility and complexity achievable in microfluidic structures [204]. The manufacture of microfluidic chips in particular. Currently, microchannels are created on silicon or glass substrates using photolithography and soft lithography, which are then replicated onto PDMS [205, 206]. Nonetheless, producing PDMS moulds through photolithography is still time-consuming and costly [207]. In recent years, DLP 3D printing has emerged as a next-generation technique for printing complex 3D architectures with micro-scale resolution; it offers superior speed, resolution, scalability, and flexibility compared to traditional methods [208]. Researchers are exploring

the potential of DLP technology for microfluidics to advance research and development in molecular diagnostics and research biology.

To demonstrate how a DLP printing system can print microfluidic chips, Shallan et al. [209] demonstrated the printing of microfluidic chips using a commercial DLP 3D printer (Miicraft, Hsinchu, Taiwan). Using a one-step exposure method based on DLP technology and Spot-E elastic resin, Büttner et al. [210] have successfully fabricated inertial microfluidic devices with intricate channel geometries. Microscopic characterisation revealed that these channels exhibited varying heights ranging from 25 to 150 μm. Macdonald et al. [211] used Fused Deposition Moulding (FDM), Polyjet, and DLP-SLA technologies to print Y-junction microfluidic chips. By utilising surface profilometry and scanning electron microscopy (SEM) characterisation techniques, the DLP-SLA-printed microfluidic chips showed the smallest channel size (154 ± 10 μm) and the least roughness values (Ra = 0.35 μm). van der Linden et al. [212] optimised the microfluidic design and a desktop DLP Printer to print the microfluidic chip within 15 min. Unlike PDMS, PMMA and other conventional elastomers and thermoplastics, hydrogel-based microfluidic chips are attracting increasingly more research attention. Microfluidic chips could be valuable in rapidly integrating micro-tissue models into organs-on-chips and high-throughput drug screening platforms. Weigel et al. [189] proposed photopolymer resins for a high-resolution DLP printing system, which consisted of 2-phenoxy ethyl acrylate (POEA), 20% (w/w) 1,3,5-triallyl-1,3,5-triazine-2,4,6(1H,3H,5H)-trione (TATATO), 0.1% (w/w) TPO and 0.225% (w/w) Sudan I to fabricate flexible microfluidic devices. Bhusal et al. [213] developed a multi-material DLP printing system to print hydrogel with a microfluidic chip (Figure 12a), which consisted of a synthetic composite hydrogel bio-ink consisting of PEGDA and GelMA and fabricated different microfluidic chips with various project patterns (Figure 12b).

However, the challenges of microfluidic chips based on DLP technologies are precisely controlling the penetration of light energy to print channel structures. The UV light will penetrate the previously printed layers when the DLP 3D printer cures the subsequent layers. UV light irradiation could photopolymerise the resin inside the microfluidic inner channel, causing blockage and limiting monolithic-size microfluidic chips' minimum inner dimensions [214, 215]. Gonghua et al. [216] utilised a synthetic polymer based on PEGDA as the monomer to print microfluidic channels (60 μm × 108 μm) via DLP technology. Meanwhile, Gong et al. [152] introduced a custom-designed digital light

processor stereolithographic (DLP-SLA) 3D printer, along with a novel mathematical model aimed at accurately quantifying the optical penetration depth of the resin. The researchers conducted comprehensive characterisation using SEM and optical microscopy techniques to validate the flow channels with widths below 25 μm and heights of 3 mm successfully printed.

Numerous approaches have been proposed to achieve precise control and printing of microfluidic channels with high accuracy. One approach involves finding suitable print parameters during printing [217]. Another method involves incorporating photo-absorber materials into the polymer system to reduce UV light penetration [218, 219], thereby decreasing resin penetration at the UV light source wavelength. However, these two methods generally lead to channel heights exceeding 100 μm or result in coloured printed structures, making it challenging to observe fluid flow under a microscope. Building upon the theoretical model of DLP, the third category utilises mathematical models to predict the thickness of the over-cured layer or optimise the process model to print microfluidic chips. Recently, Xu et al. [220] optimised the printing process using the 'bonding' method, successfully achieving high Z-resolution (within 10 μm) and high accuracy (within 2 μm) with a custom DLP 3D printing system (Figure 12c). As shown in Figure 12(d), the channels print was partially cleaved with the help of Aux e, thereby effectively preventing UV light from penetrating the channel and resulting in excessive curing and successfully printing the microfluidic channels (Figure 12e). However, it is important to note that this method is only suitable for the 'Bottom to Up' method, as the 'Top to Down' method cannot print microfluidic chips. When using DLP 3D printing to produce microfluidic chips, it is crucial to carefully consider various factors, including how to achieve large-scale printing while maintaining high resolution, precisely controlling the height and width of the microchannel, and establishing the relationship between process parameters and over-cured thickness and width for high-resolution microfluidic printing.

In DLP high-precision printing, achieving accurate fabrication of the minimum feature sizes is paramount in realising the precision printing of micro-scale structures. The dimensional characteristics of these minimum features can exert direct control over the functionality and overall performance of the final printed structure. However, attaining precise fabrication of such minute dimensions presents a multifaceted engineering challenge within the domain of DLP printing for micron-scale structures. Several interrelated factors influence this challenge:
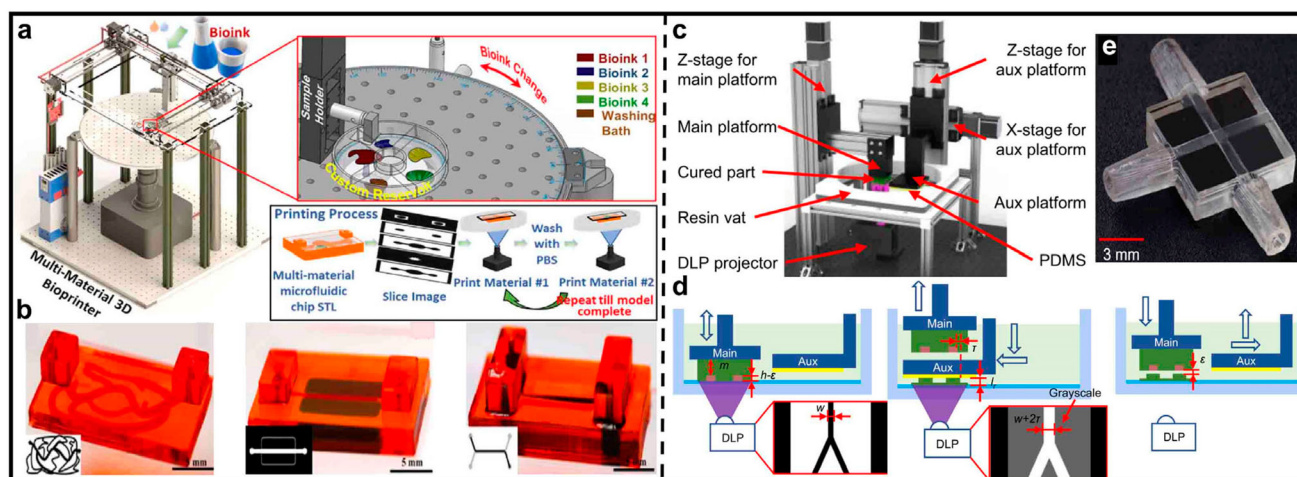
Figure 12. 3D-printed microfluidic chips based on DLP technology. (a) Schematics of the multi-material DLP printer and the fabrication process proposed for a hydrogel-based microfluidic chip. (b) Microfluidic chips are fabricated with different patterns, reprinted by permission from [213]. (c) The homemade DLP 3D printer. (d) Fabrication of the channel roof using the aux platform and the corresponding grayscale mask image. (e) Fabrication result of the microfluidic valve. Reprinted by permission from [213].

- **DLP printing system:** DLP printing systems are instrumental in achieving high-precision printing, wherein the resolution of the DMD is a crucial determinant of the minimum feature size. Concurrently, the role of the internal light source and optical system within the DLP printing system is critical in attaining exceptional precision. The Projection contrast and distortion of the optical system significantly impact project accuracy [221–223]. High-contrast optics are crucial in reducing feature edge blurring and ensuring precise projection of small feature edges onto the photopolymer, thus enhancing print accuracy. Optical distortions may decrease projection accuracy and uneven energy distribution, consequently affecting print accuracy. Addressing these challenges, Chen et al. [224].proposed a mask graphics optimisation method based on grey-level transformation processing, resulting in improved fabrication resolution for surface exposure rapid prototyping systems. Furthermore, the integrated motorised stage governs print accuracy in the vertical direction and regulates vertical surface roughness. Hence, the DLP printing system is pivotal in determining the achievable minimum feature size, underscoring its paramount significance in high-precision fabrication.

- **Photopolymer system:** The characteristics of the photopolymer system play a pivotal role in determining and influencing the minimum printed feature size. The viscosity, absorption, etc., properties of the photopolymer directly impact the precision and capability of achieving printed accuracy. Photopolymers with lower viscosity exhibit superior flowability, enabling the seamless filling of intricate microstructures during printing, leading to higher precision and smaller feature sizes [225]. The absorption properties of the photosensitive resin are crucial in determining the efficiency of light curing. Optimal matching of absorption characteristics of photopolymer with the light source enhances the curing process, resulting in higher printing precision and the ability to achieve better minimum feature sizes [226]. In conclusion, the viscosity and absorption properties of photopolymer directly influence the accuracy of DLP printing and the capability to print the minimum feature sizes. Thoughtful selection of the appropriate type of photosensitive resin and strategic optimisation of its properties are paramount in achieving superior printing accuracy and realising improved minimum feature sizes.

- **Process parameters:** Process parameters are pivotal in achieving the desired minimum feature size in DLP printing. Precise control over parameters such as print layer thickness, light exposure time, and light intensity is essential for continuously optimising printing results and improving printing accuracy. Reducing the print layer thickness will promote the creation of smoother curves and surfaces, ultimately enhancing printing accuracy. Moreover, ensuring appropriate light exposure time and intensity is vital for thorough resin curing during the light process, leading to heightened printing accuracy and the attainment of smaller minimum feature sizes. However, maintaining a delicate balance between exposure time and light intensity is crucial, as excessively long or short exposure times can compromise print accuracy. In particular, over-curing significantly impacts print accuracy, particularly when dealing with the printing of hollow structures. Thoughtful consideration and systematic adjustment of these process parameters are essential to optimise the performance of DLP printing equipment and resin, resulting in reduced feature sizes and heightened printing accuracy.

When exploring the factors influencing DLP high-precision printing, it is particularly critical to gain a deeper understanding and effective characterisation of the features and properties of printed structures. A diverse range of microscopy and surface topography analysis techniques are commonly employed in DLP high-precision printing to assess the minimum feature sizes and print quality. Optical microscopy, a non-contact measurement tool, enables observation of surface morphology and features at high resolution of the printed structures, providing detailed images and quantifying feature dimensions and shapes. SEM is invaluable for evaluating micro and nanoscale features, offering detailed morphology information through high-magnification sample surface observation. Leveraging SEM, precise measurements of minuscule feature dimensions and morphology greatly enhance print accuracy and achieve the minimum feature sizes. The 'White Light Interferometer' also effectively measures surface roughness, enabling highly accurate assessments of print surface flatness and smoothness. These measurement and characterisation methods are instrumental in obtaining precise feature sizes and comprehensively assessing print quality, further advancing DLP high-precision printing in microscale fabrication.

8 Trend of DLP towards high-precision microfabrication

## 8.1 High precision

High-precision DLP printing means that the printing system uses DMD to selectively cure the liquid resin

layer by layer, ultimately enabling the ability to print the minimum feature sizes. There are currently several factors to determine the precision of microfabrication for DLP. First, the precision of DLP microfabrication is contingent upon selecting high-resolution DMD and high-magnification projection lenses, developing high-precision photopolymer resins, and using a precise motorised stage. Optical projection systems are typically incorporated into the DLP system to achieve high projection resolution. Sun et al. [14] successfully used DLP with a 5:1 projection lens to fabricate complex 3D microstructures with a 0.6 μm feature size, while Zheng et al. [4] enhanced the resolution of the DLP system by incorporating UV reduction optics (Magnification: 6:1), leading to a final image resolution of 1.3 μm/pixel (Figure 13a).

This improved DLP system enabled the production of intricate 3D overhanging structures, including micro-lattice unit cells (Figure 13b) and porous materials (Figure 13c). Furthermore, several mature companies, including BMF, have developed high-precision DLP 3D printers with custom high-magnification projection lenses, such as the 'S130' and 'S140', which have printing resolutions of 2 and 10 μm, respectively. However, high-magnification projection lenses can induce project image distortion and low contrast, limiting the DLP system's resolution. Moreover, the resolution of the DLP system is mainly dependent on the diffraction limit of the optical system according to the 'Abbe diffraction' limit. Therefore, there exists a 'limiting projection size' for DLP projection systems, and it will not be reduced indefinitely. In addition, the research on developing photopolymer resins for high-precision DLP printing is also limited. Developing a suitable photopolymer resin requires optimising the resin components, formulations, and ratios of monomer, photo-initiator, photo-absorber, etc. A high-precision photopolymer system is critical to printing single-micron precision hydrogel 3D structures. The precision of X, Y and Z motorised stages also plays a crucial role in determining layer thicknesses and positioning accuracy in the vertical direction, thereby influencing printing precision. In DLP 3D printing, the horizontal resolution of the printing system hinges upon the high-resolution DMD and the high-magnification projection lens. Simultaneously, the vertical resolution of the print is influenced by the motorised stage, which is responsible for determining the thickness of the print layer, thereby directly impacting the final print speed and efficiency. When printing the 3D structure, increasing the layer thickness can effectively reduce the number of layers and shorten the printing time, improving printing efficiency. However, a larger print layer thickness will introduce a prominent 'step phenomenon' along the vertical direction, affecting both the surface roughness of the structure and the overall printing accuracy. Nevertheless, adopting smaller print layer thicknesses places higher demands on the 'Minimum Achievable Incremental Movement' and 'Bidirectional Repeatability Accuracy' of the motorised stage. With each motion, the stage inevitably introduces motion errors, which can accumulate as the number of layers increases, ultimately affecting the vertical accuracy of the printed structure. Furthermore, reducing the thickness of the printed
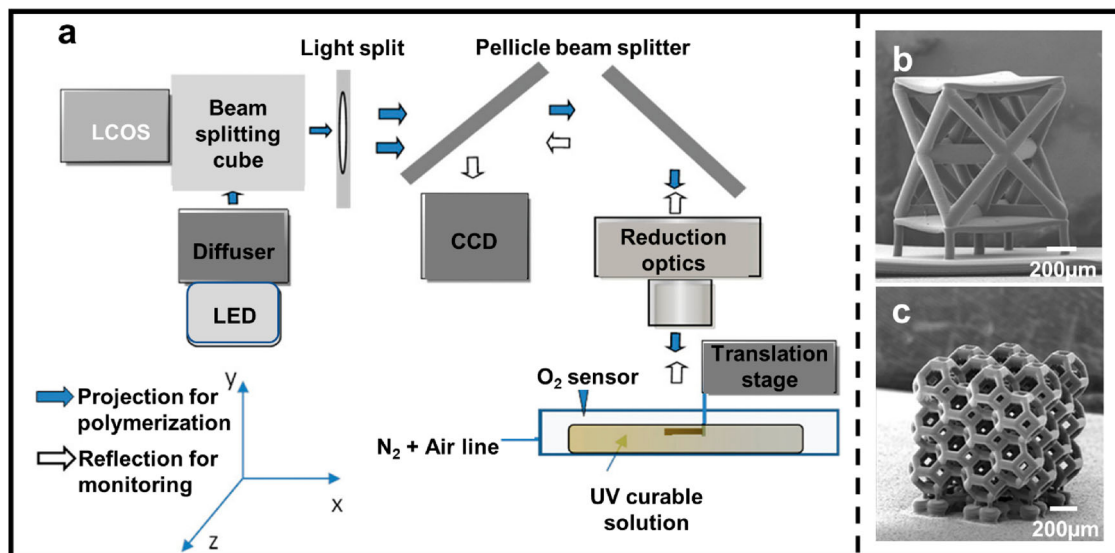
Figure 13. (a) Schematic illustration of the PμSL system, (b) Micro-lattice unit cell structure, (c) Porous structure with tetrakaidecahedron unit cell architecture Reproduced with permission from [4].

layer results in a linear increase in printing time, consequently reducing the printing efficiency. Presently, DLP commercial or laboratory printing systems can print layer thicknesses ranging from 10 to 50 μm, with some high-precision systems achieving layer thicknesses of 10 μm or less. Hence, users need to exhibit flexibility in selecting the appropriate layer thickness to strike a delicate balance between print resolution and speed, thereby achieving high print accuracy at the desired printing pace. Therefore, a comprehensive approach that optimises the motion, photopolymer, and projection systems is essential for obtaining high-precision printing results and improving the overall accuracy of microfabrication. Therefore, a comprehensive approach to optimising machine, resin, and projection systems is necessary to improve overall precision in microfabrication.

8.2 Large-area printing

Achieving large-area printing with high resolution is a significant challenge for advanced DLP printing systems, particularly in applications like microstructure fabrication, requiring a relatively large printing area. Although polymers with high-resolution three-dimensional micro-architectures offer numerous mechanical, energy conversion, and optical benefits. However, the printing area significantly hampers the applications of high-precision 3D microarchitectures. Consequently, exploring ways of achieving large-area printing with high resolution is essential. Several techniques have been proposed.

- **Motorised stage:** Motorised stage technology is classified into two main categories: digital light engine moves and build platform moves. Digital light engine translation involves fixing the digital light engine on a motorised stage, which moves along the $X–Y$ axis to enable large-scale printing. In 2002, Smith et al. [227] tried to fix a digital light engine on a motorised stage with the $X–Y$ translation. The digital light engines along the X/Y axis correspond to the motorised stage to get large-scale printing (Figure 14a). The build platform translation is currently the dominant method used on commercial printers such as BMF and Nanofabrica, offering better stability of projection images during printing. Compared to digital light engine translation, fixing the build platform on the motorised stage is more stable and provides better stability of projection images during the printing (Figure 14b). However, in addition to the limitations imposed by the X/Y motorised stage range, implementing motorised

stage stitching to enable large-area printing introduces the possibility of 'Bidirectional Repeatability' errors. These errors can lead to overlapping or gapped regions, significantly impacting print accuracy. Although image processing algorithms can help mitigate some of these errors, the challenge of minimising stitching errors remains.

- **Multi-Projector:** As shown in Figure 14(c), a multi-projector is based on arranging multiple projectors, and each projector covers a smaller image of the printing platform [228]. However, this method has not gained widespread popularity due to its high cost and gaps between each projector projection area.

- **Multi-degree of freedom mechanism:** In 2016, Wu et al. [229] incorporated the Delta mechanism into the DLP printing system to facilitate large-area printing. This multi-degree mechanism enables the build platform to move vertically along the z-axis and rotate horizontally while holding the cured models (Figure 14d). However, using squares to cover rectilinear polygons is challenging since most practical approximation algorithms are designed to handle only rectilinear or orthogonal polygons. Thus Delta technology has not been widely employed due to its algorithms' complexity and limited universality [231]. Additionally, implementing large-area printing with Delta requires complex control procedures, and a comprehensive algorithm is also a significant limitation for its development. As a result, there are currently only a few applications of the DLP large-area printing technique using the multi-degree of freedom mechanism.

- **Scanning mechanism:** Researchers have also attempted to combine scanning mechanisms from laser-based stereolithography with the DLP printing system to achieve large-area printing. The scanning mechanism involves using a galvanometric mirror as the scanning optics, where every projection area acts like one pixel and projects into the photopolymer resins (Figure 14e) [230]. This system allows the fabrication of high-precision microstructures with feature sizes exceeding four orders of magnitude (Figure 14g) and printing precision to single-micron accuracy (Figure 14f). However, positional errors may be introduced using a scanning mechanism like the motorised stage stitching method. Therefore, the scanning mechanism combines with DLP. Although it proposes a new idea to get large-area printing, the technology is not yet very mature and needs to be optimised. In 2023, Xu et al. [232] introduced a novel and efficient approach called hopping light (HL) for achieving large-area printing. The method involves leveraging the reverse rotation of 'Galvo
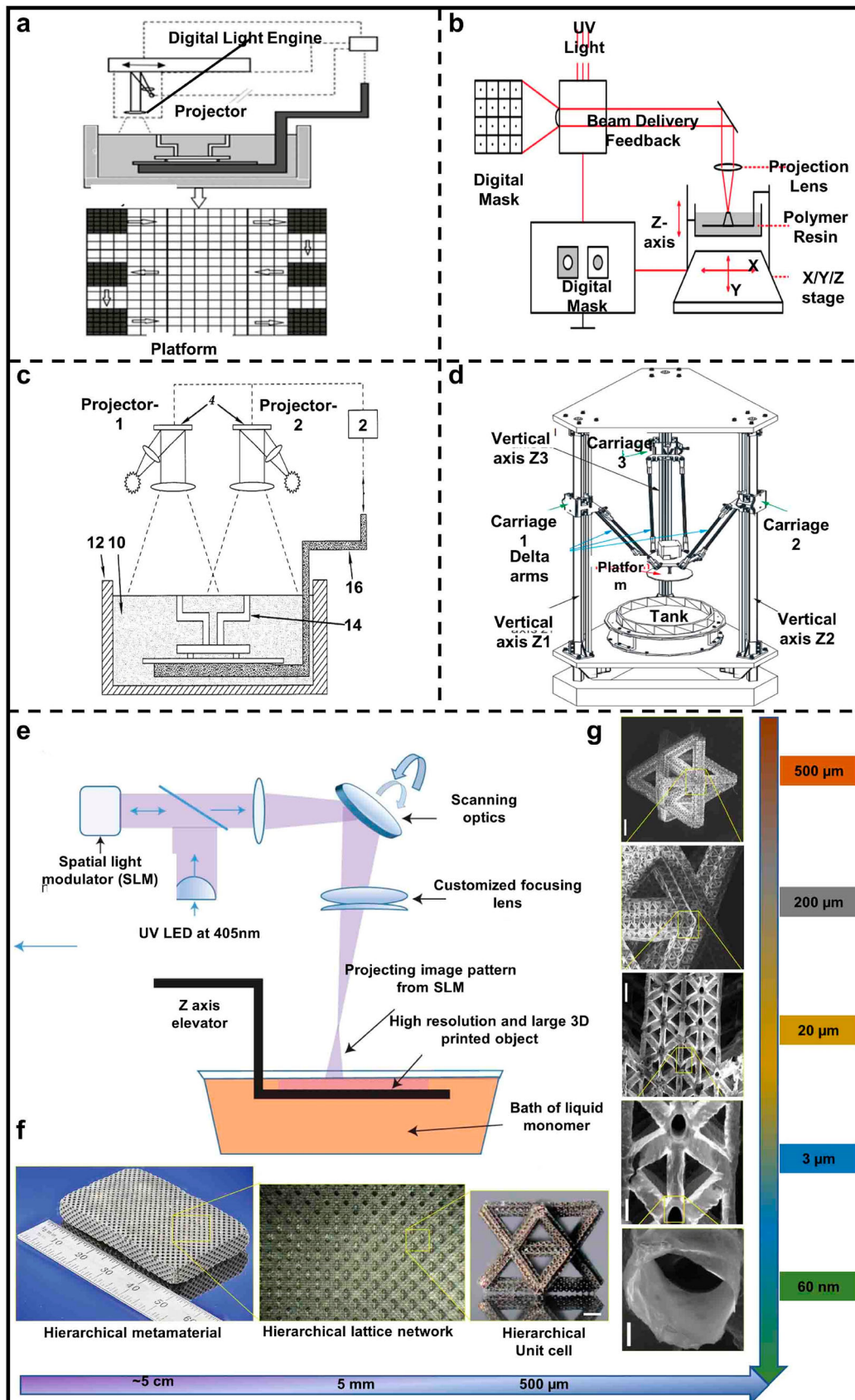
Figure 14. (a) Large-scale mask projection by moving projectors, reproduced from [227]. (b) Large-scale printing projection by moving platforms. (c) Prototype of a delta DLP 3D printer, reproduced from [228]. (d) The Delta mechanism to realise large-scale print, reproduced from [229]. (e) The large-area DLP printing system. (f) Optical microscope images of bulk hierarchical lattice material with a network of hierarchical stretch-dominated octet unit cells. (g) Scanning electron micrographs of the hierarchical structure cross-section of multiscale metamaterial unit cell, reproduced by permission from [230].

mirrors' and the movement of the image in each cycle. By utilising the fast-rotating capability of the 'Galvo mirrors', a new cycle is initiated, enabling the realisation of large-area prints. The HL technique demonstrates high printing speed and coverage efficiency, offering a promising solution for overcoming the limitations associated with conventional printing methods.
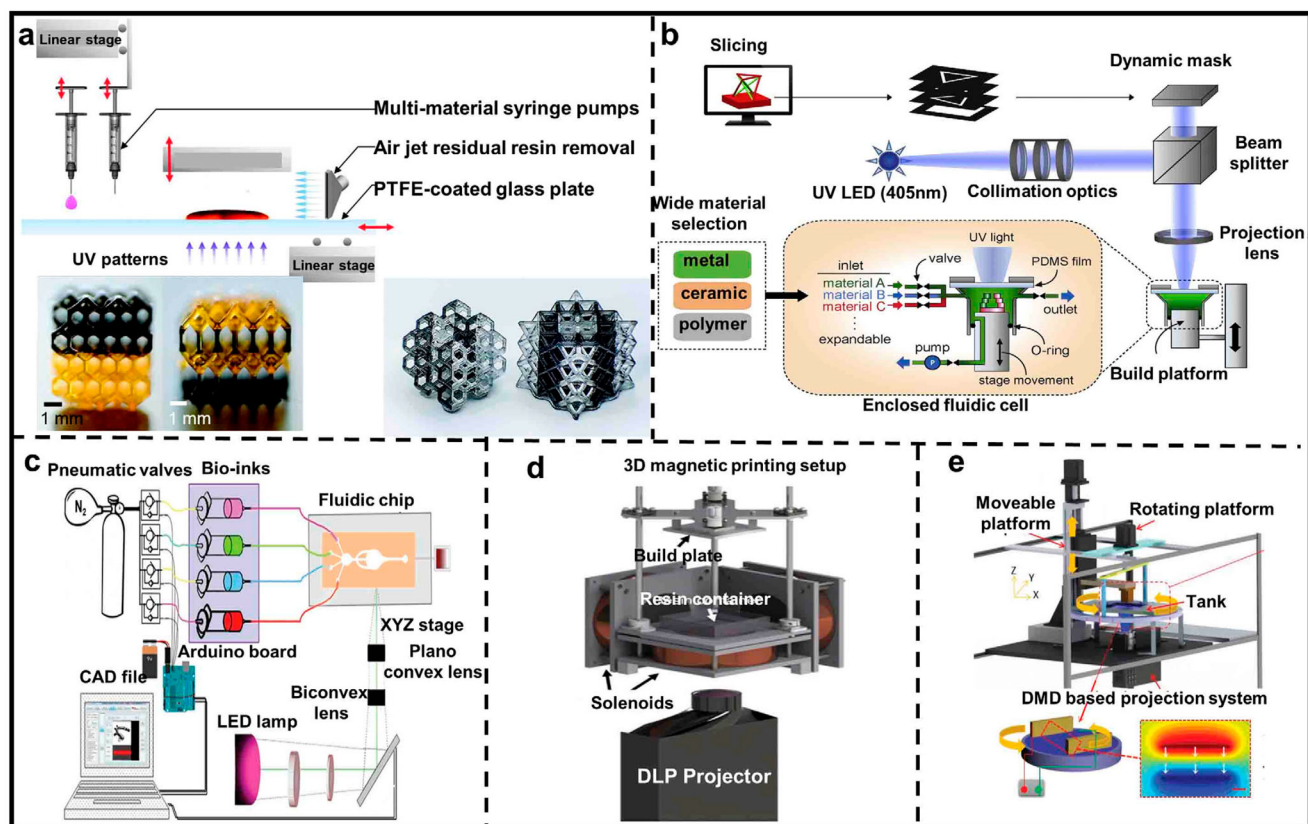
8.3 Multi-material printing

DLP is predominantly utilised in single-material printing as an exact microfabrication technique. Nonetheless, the exigencies of sophisticated printing necessitate the use of multiple materials simultaneously. The increasing demand for multi-material 3D printing has brought challenges that must be addressed. The main challenge is effectively removing residual resins from the printed structure and preventing mutual contamination. The research community has responded by proposing six main approaches for multi-material printing.

- Rotating Vat Carousel System: In 2004, Wicker et al. [233] designed a multi-vat carousel system based on a commercial 3D printer inspired by the microscope converter to enable multi-material printing via DLP technology. However, the spatial constraints imposed by the multiple vats limited the system. In 2006, Wicker et al. [13] developed a new rotating vat carousel system, which featured an enhanced platform assembly and a multi-pump filling/levelling mechanism. In 2009, Jae and Wicker et al. [15] introduced a syringe pump subsystem for controlling the dispensing of materials into the build vat, thereby strengthening the system's multi-material printing capabilities. Subsequently, in 2011, Wicker et al. [16] further improved the switching efficiency and minimised material contamination by developing an automatic levelling system and an improved rotating vat carousel system. Despite these advancements, the cleaning pool used in the multi-material printing process was frequently reused, leading to mutual contamination between the resins and reduced printing efficiency. Additionally, changing resins necessitated turning the rotating vat, which further lowered printing efficiency. Thus, while this approach addressed the issue of multi-material printing, its practical applicability remained limited.
- Air-Jet: In 2018, Ge, Qi et al. developed a novel DLP printing system. [24]. A new minimal-waste material exchange mechanism was proposed by utilising an air jet system that involves a borosilicate glass plate coated with optically clear PTFE, which avoids cross-contamination during multi-material printing (Figure 15a). This innovation eliminated the need for cumbersome procedures and resulted in a 58% increase in printing efficiency compared to existing studies that employed cleaning solutions. Remarkably, the air-jet cleaning method applied a pressure of 0.5 MPa, which could potentially cause damage to soft materials such as hydrogels and other polymer systems. This method is only suitable for resins with high mechanical strength since soft living cells and encapsulation hydrogels may be adversely affected. Moreover, in 3D bioprinting, the 'Air-Jet' method may not be used for high-precision fabrication. Nonetheless, the proposed approach effectively avoids contamination by different resins in multi-material printing.
- Microfluidic dispensing: The precise control of droplet size in microfluidic chips presents an opportunity to mix or extract multiple materials. Exploiting this potential, Amir et al. [25] integrated a microfluidic platform into a DLP printing system, as shown in Figure 15(b). The authors demonstrated successful printing of a rat vasculature network using GelMA and PEGDA polymers, thereby confirming the viability of multi-material printing with an integrated microfluidic platform. However, the use of microfluidic chips does not fully mitigate the risk of multi-material contamination, and the narrow inner diameter of the chip channel during material change can lead to inefficient extrusion of resin. These challenges present limitations for the widespread use of multi-material printing.
- Pump transfer system: Extrusion-based technology has been extensively used in multi-material 3D printing. In 2019, Han et al. [234] developed a rapid printing system for multiple materials, including valves, pumps and outlets, to control the printing process precisely. The developed system allows the fabrication of complex metallic, ceramic, and biomedical structures by switching between micro- and nanoparticle suspensions during printing (Figure 15c). While this printing approach effectively addresses the challenge of multi-material printing, the pump transfer system does not completely prevent material contamination during the printing process with multiple materials.
- Magnetic and electric field excitation: Magnetic and electric fields provide another means of controlling material behaviour during multi-material 3D printing [235]. The system employs a magnetic field to control the direction of ceramic-reinforcing particles and print ceramic/polymer composites (Figure 15d).

Figure 15. Multi-material printing system based on the DLP technology. (a) The schematic of multi-material printing based on the air jet cleaning system and printing structures Reproduced with permission from [15]. (b) Schematic illustration of the multi-materials printing based on pump system, reproduced permission from [234]. (c) Schematic illustration of the multi-materials printing based on microfluidic ship system, reproduced with permission from [25]. (d) Schematic illustration of the multi-materials printing based on the magnetic printing system, reproduced from [235]. (e) Schematic illustration of the multi-materials printing based on the electrically assisted 3D printing device, reproduced by permission from [236].

Similarly, Yang et al. [236] employed a rotating electrical field to align multi-walled carbon nanotubes (MWCNTs) dynamically. To control the orientation of the MWCNTs, DC voltages were applied on two parallel plate electrodes, generating a parallel electric field (Figure 15e). The team successfully printed an artificial meniscus and nacre-inspired hierarchical structures. Although magnetic and electric field excitation methods are applicable only under specific circumstances and for custom applications, they offer a valuable approach to high-precision multi-material printing.

• Centrifugal multi-material printing: Ge, Qi et al. [237] have presented a centrifugal multi-material (CM) 3D printing method based on DLP technology that generates large-area, multi-material 3D structures. Using centrifugal force, non-contact and high-efficiency multi-material switching is achieved, enabling the CM 3D printer to print heterogeneous 3D structures in large areas (up to 180 mm × 130 mm) using various materials, including hydrogels, functional polymers, and ceramics. The modulus of the printed material can span a wide range of eight orders of magnitude (from 103 to 1011 Pa), and up to four different resins can be printed. However, the minimum achievable print feature size using the CM printing method is limited to 500 μm, which falls short of the requirements for high-precision microfabrication. Therefore, print accuracy remains a major constraint for the promotion of CM printing.

8.4 High-speed printing

As a rapid prototyping technology, how to achieve high-precision fabrication and high-speed printing has constrained the development of DLP. Since the first proposal of DLP today, there has been non-stop research and innovation to achieve faster printing. Significant progress has been made to attain fast printing, and some good designs have been successfully implemented in commercial printers, further expanding the scope of DLP printing. The following discussion focuses on such high-speed printing:

CLIP: In 2015, Tumbleston et al. [22] introduced the Continuous Liquid Interface Production (CLIP) concept, which utilised Teflon film to generate an 'oxygen-containing dead zone'. This approach was predicated on inhibiting oxygen in free-radical polymerisation, employing an oxygen-permeable window [21]. The dead zone thickness in Teflon film was around 20 μm, allowing printing speeds to exceed 300 mm/hour. Implementing the dead zone design dramatically improved printing speed, enabling the production of parts within minutes instead of hours. However, this method's high-speed printing capability may come at the cost of reduced accuracy, as the actual print accuracy is around 70 μm.

CAL: Layer-by-layer printing may have limitations in terms of printing efficiency. In 2017, Shusteff et al. [23]. proposed the use of volumetric build setups to fabricate intricate millimetre-scale structures through holography (Figure 16b). A proposed method involves using three orthogonally directed light beams intersecting and superimposing to compensate for the limited axial resolution from the other beam directions. In 2019, Kelly et al. [26] presented a manufacturing technique for achieving volumetric photopolymerisation, computed axial lithography (CAL). This method involves rotating a photopolymer in a dynamically evolving light field, as Figure16(c) shows. Bernal et al. [27] demonstrated the ability of 3D bioprinting with CAL (Figure 16d). They connected a cell-laden gel resin reservoir to a rotating platform and printed trabecular bone models with embedded angiogenic sprouts and meniscal grafts (Figure 16e). The CAL technology was then employed to project pictures with rotational angles and a 405-nm UV light source. After washing away the unpolymerised material, the recovered cellularised construct had over 85% cell viability. Toombs et al. [238] combined microscale CAL with a photopolymer-silica nanocomposite to fabricate optical components, truss and lattice structures, and three-dimensional microfluidics structures. While CAL exponentially increases print speed and enables high-speed printing, it also sacrifices some print accuracy.

HARP: The utilisation of a 'dead zone', a thin Walker et al. proposed an alternative approach that utilises a mobile liquid interface in conjunction with stereolithographic technology to achieve rapid printing (Figure 16f) [28]. The mobile liquid interface reduces adhesive forces, enabling faster printing. In the case of HARP, different flow speeds have demonstrated distinct slip boundaries. Using HARP, continuous vertical print rates exceeding 430 mm/h were achieved with a volumetric throughput of 100 $^{l/h}$, resulting in proof-of-concept structures made from hard plastics, ceramic precursors, and elastomers (Figure 16g). However, HARP has a print resolution of only 100 μm, making it unsuitable for precision microfabrication despite its ability to achieve fast printing over a large area. 100 $^{l/h.}$

Dual light sources polymerisation: In 2020, Regehly et al. [239] introduced the 'Xolography technology' that utilises dual-colour techniques with photo-switchable photo-initiators to induce local polymerisation within confined monomer volume by intersecting light beams of different wavelengths (Figure 16a). Successful
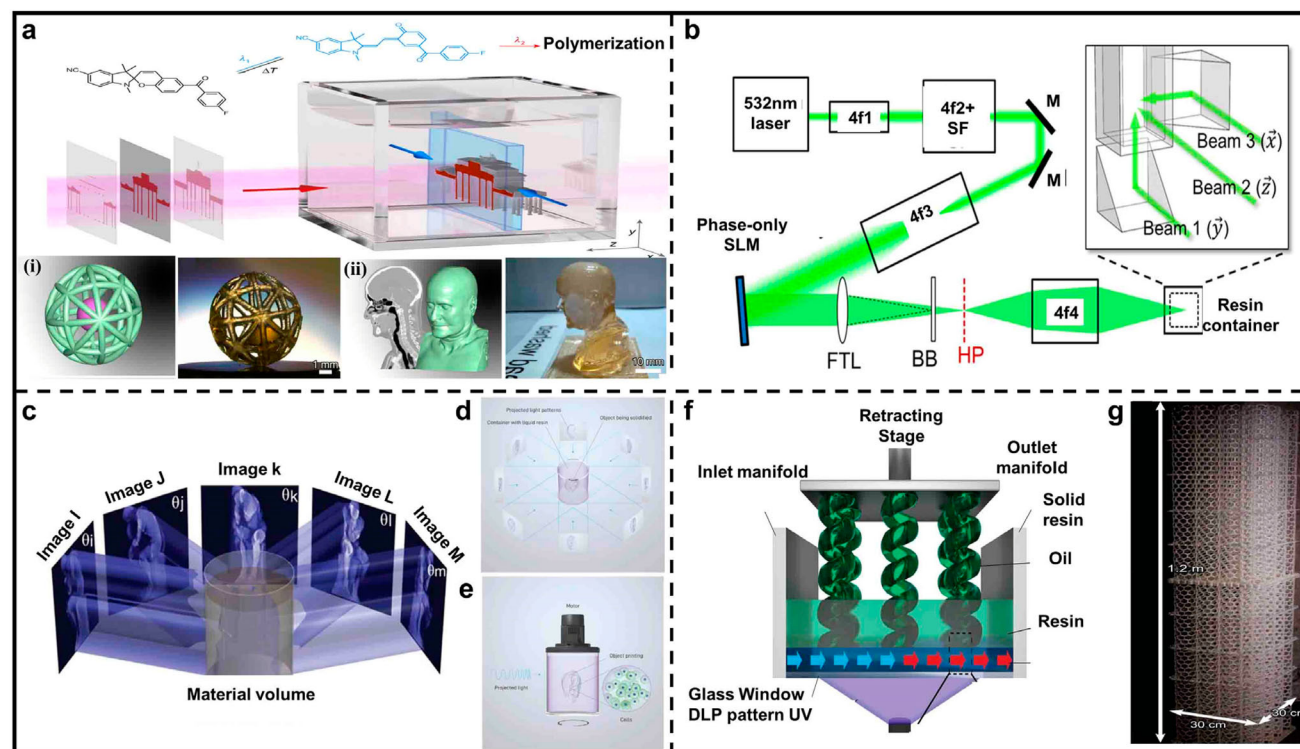
Figure 16. High-speed printing system based on the DLP technology. (a) Rendered illustration of the printing zone and associated photoinduced reaction pathways of the DCPI: (i) spherical cage with the free-floating ball, 8 mm diameters, (ii) anatomical model derived from the Manix CTA dataset, 30 mm in width, reprinted with permission from [239]. (b) Holographic volumetric 3D fabrication system schematic and example structures, repeated with permission from [23]. (c) Underlying computed axial lithography technology concept, repeated by permission from [26]. (d) Overview of the volumetric bioprinting process. (e) Schematic of tomographic projections used to print the human auricle model, repeated with permission from [27]. (f) Scheme of a 3D printed part emerging from the HARP 3D printer and rigid polyurethane acrylate lattice printed in less than 3 h (vertical print rate, 120 μm/s; optical resolution, 250 μm), repeated by permission from [28].

printing of hollowed-out solid structures (Figure 16a-i) and a human face portrait (Figure 16a-ii) has been achieved using this technology. Dual-wavelengths have enabled volumetric printing without relying on the conventional layer-by-layer stacking of vat photopolymerisation. Scott et al. [240] introduced bis[2-(chlorophenyl)−4,5-diphenylimidazole] (o-Cl-HABI), a photo-absorber to the CQ-EDAB photo-initiating system. Upon 365 nm UV irradiation, o-Cl-HABI inhibits photopolymerisation. In contrast, upon exposure to visible light (470 nm), o-Cl-HABI displays high transparency, while the CQ-EDAB photo-initiator exhibits strong absorption, allowing for efficient photopolymerisation. As a result, this technology enabled the single-step volumetric fabrication of complex objects and rapid 3D printing. However, the 'Xolography technology' resolution is approximately ten times higher than computed axial lithography without feedback optimisation. Although this technology can print with high precision and speed, it has specific photopolymer resin requirements that need to be addressed before it can be widely adopted. The final printing speed and resolution of the 'Xolography technology' are about 55 mm^3 $^{s-1}$ and 25 μm, respectively.

9 Conclusion

This review focuses on developing equipment, materials, and processing for DLP in the realm of AM. The article provides an overview of commercially available DLP printers. It evaluates the strengths and limitations of existing systems in terms of high-resolution, large-area printing, multi-material printing, and high-speed printing. The working principle and mathematical models based on photo-polymerisation under DLP are explained in detail, and the fundamental components of polymer interaction with the UV light source are elucidated. The composition of photopolymer resin is analysed using theoretical models to describe the photocuring process under DLP. In addition, the article discusses the advanced microfabrication of living materials, hydrogels, and conventional photocurable resin for microfabrication, such as microfluidic chips. Despite the rapid development of DLP printing systems, this versatile microfabrication technology still faces significant challenges in achieving high-resolution, large-area printing and multi-material printing.

- First, achieving high-resolution 3D complex microstructures requires a DLP printing system with high resolution, a suitable polymer system, and processes directed by precise mathematical model analysis. While some DLP projectors can provide a resolution

up to a single micron, UV light penetration cannot be precisely controlled, which easily causes over-cured structures. Consequently, the actual printing resolution is always worse than the theoretical one. Achieving high-precision printing in DLP technology remains a significant challenge, although future advancements promise to establish correlations between process parameters, polymer systems, and printing accuracy. Artificial intelligence (AI) presents a potential avenue for exploring such relationships and eventually enabling high-precision printing. However, attaining fine-scale printing with exceptional accuracy currently poses ongoing difficulties within DLP printing. Addressing these challenges and developing robust solutions will be essential for advancing the capabilities of DLP technology in achieving precise and intricate prints.

- Second, high-precision large-area printing is a challenging task for DLP systems. Current industrial and academic development often utilises a motorised stage to achieve high-precision, large-area printing. However, a motorised stage inevitably introduces inherent positioning errors such as bi-directional repeatability. Although some image processing algorithms, such as the grey algorithm, can compensate for the loss of stitching accuracy due to large printing areas, they use fuzzy algorithms to lose accuracy in exchange for compensation and do not substantially improve accuracy against stitching errors. Additionally, the slicing software needs to cut up many two-dimensional images and send them to DLP light engines to project on the photopolymerisation resins. However, the memory of DLP light engines is limited, and they can only store a few images. Some researchers have developed a specific software module to store these images on a third-party computer and use C language or G-code to transfer images to DLP light engines for processing. Nonetheless, this method is neither stable nor convenient. Optimising image processing and storage technologies is critical to developing an efficient DLP printing system. · Third, the inability to achieve a perfect multi-material printing system severely restricts the development of DLP printing system applications. Although various system designs are available to complete multi-material printing, such as a multi-rotational vat, combining the extrusion nozzle to deposit different materials in different boxes into a glass plate or combining with microfluidic dispensing, the design of multi-material printing remains immature. It is usually time-consuming and cannot avoid materials contamination. Qi Ge [24] proposed using air pressure to generate air to prevent this problem.

However, this method is not compatible with some hydrogels or soft polymer systems in 3D bioprinting, and it is only suitable for rigid materials with high mechanical strength. Furthermore, the cells need to be encapsulated by a hydrogel system. Therefore, developing a multi-material system that enables printing without material contamination and imposes no constraints on the choice of printing materials will be a persistent challenge in advancing DLP technology. Overcoming this challenge is paramount for expanding the capabilities and applications of DLP-based 3D printing. Lastly, the polymer system significantly influences the mechanical properties, printing resolution, and speed of DLP printing. Thus, determining the appropriate photopolymer resin compositions and corresponding concentration is crucial for high-resolution DLP printing. Commercial DLP 3D printers offer a range of custom-specific resins and related process parameters. However, customers who want to print complex microstructures can only use the proprietary resins provided by the suppliers. This is particularly problematic for research, as the material system and process are not open. Developing new materials, such as nanomaterials printing, gradient materials printing, drug printing, intelligent materials printing and determining materials, requires significant effort to achieve the optimal process for high-precision, high-resolution printing of microstructures. AI will play a pivotal role in printing materials in the future, as the process determines if the material's properties and process characteristics can be extracted well.

In conclusion, we contend that DLP 3D printing represents a highly versatile and capable AM technology for micro-scale fabrication, offering high-precision, large-area, and multi-material capabilities. Industrial-scale DLP systems have already demonstrated their ability to fabricate microdevices with remarkable precision, and we anticipate continued progress in developing living materials, soft polymers, and functional nanomaterials. Further advances in DLP printing will rely on improved high-precision image stitching, multi-material switching, and process optimisation. AI-driven process optimisation is one promising avenue for exploring the printing of multi-scale features, ranging from single to hundreds of micrometres, with high precision.

Acknowledgements

Disclosure statement

Funding

Data availability statement

There is no data set associated with this paper.

Notes on contributors

Xinhui Wang is a PhD student in manufacturing and design at the School of Mechanical and Materials Engineering at University College Dublin (UCD) in Ireland. His research interests include additive manufacturing, micron manufacturing and 3D bioprinting. Application areas: organ-on-a-chip, microfluidic chip, biomedical devices.

Nan Zhang is an assistant professor in manufacturing and design at the School of Mechanical and Materials Engineering at University College Dublin (UCD) in Ireland. His research covers polymer micro/nano manufacturing, precision manufacturing of plastic microfluidic chips, microfluidic systems for synthesising genetic nanomedicine and molecular diagnostics, manufacturing functional micro/nano structured surfaces, and atomic and close-to-atomic-scale manufacturing. He won 4.5 million grants in his early career and has published many peer-reviewed journal papers in *Materials Today, Nano Letters, ACS Applied Materials and Interface and the International Journal of Machine Tool and Manufacture*. He was the chair of the 6th and 8th international conferences on polymer replication on the nanoscale (PRN2019, PRN2022). He is the associate editor of the journal 'Frontier in Lab on a Chip Technologies' and a Board member of the Microfluidic Association. His research has generated several patents which have been commercialised or are in the process of being commercialised.

Jinghang Liu has spent 3 years as a senior engineer and 6 years as an academic researcher, working in both industrial and academic settings. Now, she is an assistant lecturer at Technological University Dublin. She has 3 years of industrial experience in biomedical instrument development and as a leader to develop a novel biomedical platform for patient-derived therapeutics for cancer treatment. Her work resulted in 20

publications across reputable journals, conferences and book chapters, with a citation count of 429, gaining recognition within the academic community.

Yang Zhang is a senior researcher at the Technical University of Denmark, and she is an experienced researcher with a demonstrated history of working in research and industry. She was skilled in Polymer injection moulding, Surface Metrology, Polymers, Laser Processing and Project Management. Strong research professional with a PhD in Manufacturing Engineering from the Technical University of Denmark.

Aminul Islam is an associate professor at the Centre for Acoustic Mechanical Micro Systems (CAMM), Technical University of Denmark (DTU). Since 2008, he has been heavily involved in scientific research in multi-material micro-manufacturing. He has an excellent mixture of research experience both from industry and academia. I am specialised in micro/anon and precision manufacturing. At the same time, I am an experienced project manager having experience with different national and international projects. My research interest includes Advanced materials and process technologies for micro/nano-manufacturing and Additive manufacturing of smart structures and functional surfaces.

Per Magnus Kristiansen is a full professor in engineering at the FHNW University of Applied Sciences and Arts Northwestern Switzerland. He is also the head of the Institute of Polymer Nanotechnology (INKA). His research topics include 'Additive manufacturing on the micro – and nanoscale', and 'Micro – and nanostructuring of polymer surfaces'.

Michael Gilchrist is a full professor in manufacturing and design at the School of Mechanical and Materials Engineering at University College Dublin (UCD) in Ireland. His leadership roles have included 7 years as Head of the UCD School of Mechanical & Materials Engineering (2011–18), and 3 years as VP for Research in UCD's College of Engineering, Mathematical & Physical Sciences (2009-11). His research concerns non-linear materials' dynamic mechanical behaviour, including biological tissue and polymer materials. Intellectual property from his research has been licensed to 10 separate research groups and companies in Ireland, the UK, Belgium, the USA, Canada and Singapore. He has been the lead PI on in excess of €10m of competitively won research funding. He holds a visiting professorship at the University of Ottawa and has previously been a visiting professor at CNRS & ENSAM-Paris (2003-4).

References

[1] Melchels FP, Feijen J, Grijpma DW. A review on stereolithography and its applications in biomedical engineering. Biomaterials. 2010;31(24):6121–6130. doi:10.1016/j.biomaterials.2010.04.050

[2] Ge Q, Li Z, Wang Z, et al.. Projection micro stereolithography based 3D printing and its applications. Int J Extreme Manuf. 2020;2:2. doi:10.1088/2631-7990/ab8d9a

[3] Quan H, Zhang T, Xu H, et al. Photo-curing 3D printing technique and its challenges. Bioact Mater. 2020;5(1):110–115. doi:10.1016/j.bioactmat.2019.12.003

[4] Zheng X, Deotte J, Alonso MP, et al.. Design and optimization of a light-emitting diode projection microstereolithography three-dimensional manufacturing system. Rev Sci Instrum. 2012a;12:125001. doi:10.1063/1.4769050

[5] Lee K-S, Kim RH, Yang D-Y, et al. Advances in 3D nano/microfabrication using two-photon initiated polymerization. Progr Polymer Sci. 2008;33(6):631–681. doi:10.1016/j.progpolymsci.2008.01.001

[6] Darkes-Burkey C, Shepherd RF. High-resolution 3D printing in seconds. Nature. 2020;588(7839):594–95. doi:10.1038/d41586-020-03543-3.

[7] Hull C. F. P. m. p.-p. (resin)-SLA, 1986.

[8] Hornbeck, L. J. (29 Oct. 1991). U. S. Patent.

[9] Bertsch A. Microstereophotolithography using a liquid crystal display as dynamic mask-generator.pdf. Microsyst Technol. 1997;3(2):42–47. doi:10.1007/s005420050053.

[10] Beluze L. Microstereolithography a new process to build complex 3D objects, 1999.

[11] Shoji Maruo KIaTN. Multi-polymer microstereolithography for hybrid opto-MEMS.pdf. IEEE, 2001.

[12] G W. Digital micromirror device based microstereolithography for micro structures of transparent photopolymer and nanocomposites, 2003.

[13] Wicker AIR. Development of an automated multiple material stereolithography machine. 2006.

[14] Sun C, Fang N, Wu DM, et al. Projection micro-stereolithography using digital micro-mirror dynamic mask. Sensors Actuat A Phys 2005; 1:113–120. doi:10.1016/j.sna.2004.12.011.

[15] Choi W,R. Multi-material microstereolithography. Int J Adv Manuf Technol. 2009;5-8:543–551. doi:10.1007/s00170-009-2434-8.

[16] Wicker R. Multi-material stereolithography. J Mater Process Technol. 2011;3:318–328. doi:10.1016/j.jmatprotec.2010.10.003

[17] B9Creations. https://tracxn.com/d/companies/b9creations/__iNXQYOQtobKhLI1S10wagHhhGRNuLFKdCrM-Y_O1fds, 2012.

[18] Zhou C, Chen Y, Yang Z, et al. Digital material fabrication using mask-image-projection-based stereolithography. Rapid Prototyping J. 2013;3:153–165. doi:10.1108/13552541311312148

[19] Ge Q, Qi HJ, Dunn ML. Active materials by four-dimension printing. Appl Phys Lett. 2013;103:13. doi:10.1063/1.4819837

[20] Zheng X, Lee H, Weisgraber TH, et al. Ultralight: ultrastiff mechanical metamaterials. Science. 2014;6190:1373–1377. doi:10.1126/science.1252291.

[21] Janusziewicz R, Tumbleston JR, Quintanilla AL, et al. Layerless fabrication with continuous liquid interface production. Proc Natl Acad Sci USA. 2016;113(42):11703–11708. doi:10.1073/pnas.1605271113

[22] Tumbleston JR. Continuous liquid interface production of 3D objects. Science. 2015;347(6228):1349–52. doi:10.1126/science.aaa2397.

[23] Shusteff M, et al. One-step volumetric additive manufacturing of complex polymer structures. Sci Adv. 2017;3(12). doi:10.1126/sciadv.aao5496.

[24] Kowsari K, Akbari S, Wang D, et al. High-efficiency high-resolution multimaterial fabrication for digital light processing-based three-dimensional printing. 3D Print Add Manuf . 2018a;3:185–193. doi:10.1089/3dp.2018.0004

[25] Miri AK, Nieto D, Iglesias L, et al. Microfluidics-enabled multimaterial maskless stereolithographic bioprinting. Adv Mater. 2018;27:e1800242. doi:10.1002/adma.201800242

[26] Kelly BE, et al. Volumetric additive manufacturing via tomographic reconstruction. Science. 2019;363 (6431):1075–1079. doi:10.1126/science.aau7114.

[27] Bernal PN, Delrot P, Loterie D, et al. Volumetric bioprinting of complex living-tissue constructs within seconds. Adv Mater. 2019;31(42):e1904209. doi:10.1002/adma.201904209

[28] Walker DA, Hedrick JL, Mirkin CA. Rapid, large-volume, thermally controlled 3D printing using a mobile liquid interface. Science. 2019;366(6463):360–364. doi:10.1126/science.aax1562.

[29] Kang M, Han C, Jeon H. Submicrometer-scale pattern generation via maskless digital photolithography. Optica. 2020;7:12. doi:10.1364/optica.406304

[30] Fabrication BM. (S140). https://bmf3d.com/10%ce%bcm-series-printers/.

[31] Li Y, Mao Q, Li X, et al. High-fidelity and high-efficiency additive manufacturing using tunable pre-curing digital light processing. Addit Manufac. 2019. doi:10.1016/j.addma.2019.100889.

[32] Renap K, K JP. Recoating issues in stereolithography. Rapid Prototyp J. 1995;1(3):4–16. doi:10.1108/13552549510094223.

[33] Kozhevnikov A, Kunnen RPJ, van Baars GE, et al. Investigation of the fluid flow during the recoating process in additive manufacturing. Rapid Prototyp J. 2019;26(4):605–613. doi:10.1108/rpj-06-2019-0152

[34] Santoliquido O, Colombo P, Ortona A. Additive manufacturing of ceramic components by digital light processing: a comparison between the "bottom-up" and the "top-down" approaches. J Eur Ceram Soc. 2019;39 (6):2140–2148. doi:10.1016/j.jeurceramsoc.2019.01.044

[35] Kunwar P, Xiong Z, McLoughlin ST, et al. Oxygen-permeable films for continuous additive, subtractive, and hybrid additive/subtractive manufacturing. 3D Print Addit Manuf. 2020;5:216–221. doi:10.1089/3dp.2019.0166

[36] Chockalingam K, Jawahar N, Ramanathan KN, et al. Optimization of stereolithography process parameters for part strength using design of experiments. Int J Adv Manuf Technol. 2005;29(1–2):79–88. doi:10.1007/s00170-004-2307-0

[37] Verhaagen B, Zanderink T, Fernandez Rivas D. Ultrasonic cleaning of 3D printed objects and cleaning challenge devices. Appl Acoust. 2016;103:172–181. doi:10.1016/j.apacoust.2015.06.010

[38] Aznarte, E., C. Ayranci, and A. J. Qureshi. (2017). Digital light processing (DLP) anisotropic tensile considerations. *2017 International solid freeform fabrication symposium*.

[39] Sun W-S, Chiang Y-C, Tsuei C-H. Optical design for the DLP pocket projector using LED light source. Phys Proc. 2011;19:301–307. doi:10.1016/j.phpro.2011.06.165

[40] Gu Z, Fu J, Lin H, et al. Development of 3D bioprinting: from printing methods to biomedical applications. Asian J Pharm Sci. 2020;5:529–557. doi:10.1016/j.ajps.2019.11.003

[41] Wang Y, Xue D, Mei D. Projection-based continuous 3D printing process With the grayscale display method. J Manufac Sci Eng. 2020;142:2. doi:10.1115/1.4045616

[42] Xu H, Davey AB, Wilkinson TD, et al. Performance of UV-stable STN mixtures for PL-LCDs. Mol Cryst Liquid Cryst. 2004;411(1):79–91. doi:10.1080/15421400490434810

[43] Pyo SH, Wang P, Hwang HH, et al. Continuous optical 3D printing of green aliphatic polyurethanes. ACS Appl Mater Interfaces. 2017;9(1):836–844. doi:10.1021/acsami.6b12500

[44] Jiang C, Zhang H, Song J, et al. Digital micromirror device (DMD)-based high-cycle tensile fatigue testing of 1D nanomaterials. Extreme Mech Lett. 2018;18:79–85. doi:10.1016/j.eml.2017.11.005

[45] Pan J-W, Lin S-H. Achromatic design in the illumination system for a mini projector with LED light source. Optics Express. 2011;19(17):15750–15759. doi:10.1364/oe.19.015750.

[46] Sun WS, Pan JW. Non-telecentric projection lens design for an LED projector. Appl Opt. 2017;56(3):712–720. doi:10.1364/AO.56.000712

[47] Liravi F, Das S, Zhou C. Separation force analysis and prediction based on cohesive element model for constrained-surface stereolithography processes. Comput Aid Design. 2015;69:134–142. doi:10.1016/j.cad.2015.05.002

[48] Nosonovsky M, Bhushan B. Lotus versus rose: biomimetic surface effects. In: *Green Tribology*; 2012. p. 25–40.

[49] Kowsari K, Zhang B, Panjwani S, et al. Photopolymer formulation to minimize feature size: surface roughness, and stair-stepping in digital light processing-based three-dimensional printing. Addit Manufac. 2018b;24:627–638. doi:10.1016/j.addma.2018.10.037

[50] Pan Y, Zhao X, Zhou C, et al. Smooth surface fabrication in mask projection based stereolithography. J Manufac Process. 2012;14(4):460–470. doi:10.1016/j.jmapro.2012.09.003

[51] Yeung C, Chen S, King B, et al. A 3D-printed microfluidic-enabled hollow microneedle architecture for transdermal drug delivery. Biomicrofluidics. 2019;13(6):064125. doi:10.1063/1.5127778

[52] Dendukuri D, Pregibon DC, Collins J, et al. Continuous-flow lithography for high-throughput microparticle synthesis. Nat Mater. 2006;5:365–369. doi:10.1038/nmat1617.

[53] Pan Y, Zhou C, Chen Y. A fast mask projection stereolithography process for fabricating digital models in minutes. J Manufac Sci Eng. 2012;134:5. doi:10.1115/1.4007465

[54] Wu X, Lian Q, Li D, et al. Tilting separation analysis of bottom-up mask projection stereolithography based on cohesive zone model. J Mater Process Technol. 2017;243:184–196. doi:10.1016/j.jmatprotec.2016.12.016

[55] Ribo MM, et al. Optimization of a self-peeling vat for precision vat photopolymerization setups. Eur Soc Precision Eng Nanotechnol. 2019.

[56] Andersen, F. W. (2018). *Optimization of an experimental DLP platform by construction and process studies tech*. Technical University of Denmark, Kgs. Lyngby, Denmark.

[57] Jacobs PF. (1992). Rapid Prototyping Manufacturing Fundamentals of StereoLithography by Jacobs P.F. (z-lib.org).

[58] Gong H, Beauchamp M, Perry S, et al. Optical approach to resin formulation for 3D printed microfluidics. RSC

Adv. 2015;129:106621–106632. doi:10.1039/C5RA23855B

[59] Benjamin AD, Abbasi R, Owens M, et al. Light-based 3D printing of hydrogels with high-resolution channels. Biomed Phys Eng Expr. 2019;5:2. doi:10.1088/2057-1976/aad667

[60] Swineharf, D. F. (1962). Beer-Lambert Law.doi:10.1021/ed039p333

[61] Lee JH, Prud'homme RK, Aksay IA. Cure depth in photopolymerization: experiments and theory. J Mater Res. 2011;12:3536–3544. doi:10.1557/jmr.2001.0485

[62] Bennett J. Measuring UV curing parameters of commercial photopolymers used in additive manufacturing. Addit Manuf. 2017: 203–212. doi:10.1016/j.addma.2017.10.009

[63] Emami MM, Barazandeh F, Yaghmaie F. Scanning-projection based stereolithography: method and structure. Sensors Actuat A Phys. 2014;218:116–124. doi:10.1016/j.sna.2014.08.002

[64] Zhakeyev A, Zhang L, Xuan J. Photoactive resin formulations and composites for optical 3D and 4D printing of functional materials and devices. In: *3D and 4D printing of polymer nanocomposite materials, Vol. The matematic model basic of my first time*. 2020. p. 387–425.

[65] Ligon SC, Liska R, Stampfl J, et al. Polymers for 3D printing and customized additive manufacturing. Chem Rev. 2017;15:10212–10290. doi:10.1021/acs.chemrev.7b00074

[66] Carbon. (2023). https://www.carbon3d.com/about.

[67] Odian, G. (2004). *Principles of polymerization*. John Wiley & Sons. doi:10.1002/047147875x

[68] Wu J, Zhao Z, Hamel CM, et al. Evolution of material properties during free radical photopolymerization. J Mech Phys Solids. 2018;112:25–49. doi:10.1016/j.jmps.2017.11.018

[69] Shaukat, U., Rossegger, E., & Schlogl, S. (2022). A review of multi-material 3D printing of functional materials via vat photopolymerization. *Polymers (Basel)*, *14*(12). doi:10.3390/polym14122449

[70] Braunecker WA, Matyjaszewski K. Controlled/living radical polymerization: features,: developments, and perspectives. Progr Polymer Sci. 2007;32(1):93–146. doi:10.1016/j.progpolymsci.2006.11.002

[71] Chen M, Zhong M, Johnson JA. Light-controlled radical polymerization: mechanisms,: methods, and applications. Chem Rev. 2016;116(17):10167–10211. doi:10.1021/acs.chemrev.5b00671

[72] Mota C, Camarero-Espinosa S, Baker MB, et al. Bioprinting: from tissue and organ development to in vitro models. Chem Rev. 2020;19:10547–10607. doi:10.1021/acs.chemrev.9b00789

[73] Ba´rtolo, P. J. *Stereolithography: materials,: processes and ApplicationsStereolithography*. MaterProc Appl. 2011:1–36. doi:10.1007/978-0-387-92904-0_1.

[74] Tang, Y. Stereolithography cure process modeling, Georgia Institute of Technology.pdf, 2005.

[75] Zhang J, Xiao P. 3D printing of photopolymers. Polymer Chem. 2018;9(13):1530–1540. doi:10.1039/c8py00157j

[76] Brandon V. Slaughter SSK, Fisher OZ, Khademhosseini A, et al. Hydrogels in regenerative medicine. Adv Mater. 2009: 32–33.

[77] Liu Tsang V, Chen AA, Cho LM, et al. Fabrication of 3D hepatic tissues by additive photopatterning of cellular hydrogels. FASEB J. 2007;21(3):790–801. doi:10.1096/fj.06-7117com

[78] Yanan Du EL, Ali S, Khademhosseini A. Directed assembly of cell-laden microgels for fabrication of 3D tissue constructs. National Acad Sci. 2008;105(28):9522–27. doi:10.1073/pnas.0801866105.

[79] Gou M, Qu X, Zhu W, et al. Bio-inspired detoxification using 3D-printed hydrogel nanocomposites. Nat Commun. 2014;5:3774. doi:10.1038/ncomms4774

[80] Liu S, Yeo DC, Wiraja C, et al. Peptide delivery with poly(ethylene glycol) diacrylate microneedles through swelling effect. Bioeng Transl Med. 2017;2(3):258–267. doi:10.1002/btm2.10070

[81] Munoz-Pinto DJ, Jimenez-Vergara AC, Gharat TP, et al. Characterization of sequential collagen-poly(ethylene glycol) diacrylate interpenetrating networks and initial assessment of their potential for vascular tissue engineering. Biomaterials. 2015;40:32–42. doi:10.1016/j.biomaterials.2014.10.051

[82] Nichol JW, Koshy ST, Bae H, et al. Cell-laden microengineered gelatin methacrylate hydrogels. Biomaterials. 2010;31(21):5536–5544. doi:10.1016/j.biomaterials.2010.03.064

[83] Van Den Bulcke AI, et al. Structural and rheological properties of methacrylamide modified gelatin hydrogels. Biomacromolecules. 2000;1:31–38.

[84] Ahadian S, Ramon-Azcon J, Estili M, et al. Facile and rapid generation of 3D chemical gradients within hydrogels for high-throughput drug screening applications. Biosens Bioelectron. 2014;59:166–173. doi:10.1016/j.bios.2014.03.031

[85] Ahadian S, Yamada S, Ramon-Azcon J, et al. Hybrid hydrogel-aligned carbon nanotube scaffolds to enhance cardiac differentiation of embryoid bodies. Acta Biomater. 2016;31:134–143. doi:10.1016/j.actbio.2015.11.047

[86] Athirasala A, Lins F, Tahayeri A, et al. A novel strategy to engineer Pre-vascularized full-length dental pulp-like tissue constructs. Sci Rep. 2017;7(1):3323. doi:10.1038/s41598-017-02532-3

[87] Jeon O, Wolfson DW, Alsberg E. In-situ formation of growth-factor-loaded coacervate microparticle-embedded hydrogels for directing encapsulated stem cell fate. Adv Mater. 2015;27(13):2216–2223. doi:10.1002/adma.201405337

[88] Levato R, Webb WR, Otto IA, et al. The bio in the ink: cartilage regeneration with bioprintable hydrogels and articular cartilage-derived progenitor cells. Acta Biomater. 2017;61:41–53. doi:10.1016/j.actbio.2017.08.005

[89] Paul A, Manoharan V, Krafft D, et al. Nanoengineered biomimetic hydrogels for guiding human stem cell osteogenesis in three dimensional microenvironments. J Mater Chem B. 2016;4(20):3544–3554. doi:10.1039/C5TB02745D

[90] Sadeghi AH, Shin SR, Deddens JC, et al. Engineered 3D cardiac fibrotic tissue to study fibrotic remodeling. Adv Healthc Mater. 2017;6:11. doi:10.1002/adhm.201601434

[91] Shin SR, Zihlmann C, Akbari M, et al. Reduced graphene oxide-GelMA hybrid hydrogels as scaffolds for cardiac

tissue engineering. Small. 2016;12(27):3677–3689. doi:10.1002/smll.201600178

[92] Wenz A, Borchers K, Tovar GEM, et al. Bone matrix production in hydroxyapatite-modified hydrogels suitable for bone bioprinting. Biofabrication. 2017;9(4):044103. doi:10.1088/1758-5090/aa91ec

[93] Yue K, Trujillo-de Santiago G, Alvarez MM, et al. Synthesis, properties, and biomedical applications of gelatin methacryloyl (GelMA) hydrogels. Biomaterials. 2015;73:254–271. doi:10.1016/j.biomaterials.2015.08.045

[94] Zhang YS, Davoudi F, Walch P, et al. Bioprinted thrombosis-on-a-chip. Lab Chip. 2016;16(21):4097–4105. doi:10.1039/c6lc00380j

[95] Wu S, Xu R, Duan B, et al. Three-dimensional hyaluronic acid hydrogel-based models for In vitro human iPSC-derived NPC culture and differentiation. J Mater Chem B. 2017;5(21):3870–3878. doi:10.1039/C7TB00721C

[96] Lin S, Lee WYW, Feng Q, et al. Synergistic effects on mesenchymal stem cell-based cartilage regeneration by chondrogenic preconditioning and mechanical stimulation. Stem Cell Res Ther. 2017;8(1):221. doi:10.1186/s13287-017-0672-5

[97] Poldervaart MT, Goversen B, de Ruijter M, et al. 3D bioprinting of methacrylated hyaluronic acid (MeHA) hydrogel with intrinsic osteogenicity. PLoS One. 2017;12(6):e0177628. doi:10.1371/journal.pone.0177628

[98] Rossegger E, Höller R, Hrbinič K, et al. 3D printing of soft magnetoactive devices with thiol-click photopolymer composites. Adv Eng Mater. 2022;25:7. doi:10.1002/adem.202200749

[99] Cazin I, Rossegger E, Roppolo I, et al. Digital light processing 3D printing of dynamic magneto-responsive thiol-acrylate composites. RSC Adv. 2023;13(26):17536–17544. doi:10.1039/d3ra02504g

[100] Lantean S, Roppolo I, Sangermano M, et al. Magnetoresponsive devices with programmable behavior using a customized commercial stereolithographic 3D printer. Adv Mater Technol. 2022;7:11. doi:10.1002/admt.202200288

[101] Fantino E, Chiappone A, Roppolo I, et al. 3D printing of conductive complex structures with in situ generation of silver nanoparticles. Adv Mater. 2016;28(19):3712–3717. doi:10.1002/adma.201505109

[102] Gonzalez G, Chiappone A, Roppolo I, et al. Development of 3D printable formulations containing CNT with enhanced electrical properties. Polymer. 2017;109:246–253. doi:10.1016/j.polymer.2016.12.051

[103] Salas A, Pazniak H, Gonzalez-Julian J, et al. Development of polymeric/MXenes composites towards 3D printable electronics. Composites B Eng. 2023;263. doi:10.1016/j.compositesb.2023.110854

[104] Gastaldi M, Roppolo I, Chiappone A, et al. Thermochromic photoluminescent 3D printed polymeric devices based on copper-iodide clusters. Addit Manufac. 2022;49. doi:10.1016/j.addma.2021.102504

[105] Chabok H ZC, Chen Y, Eskandarinazhad A, et al. Ultrasound transducer array fabrication based on additive manufacturing of piezocomposites. Int Symp Flexible Autom. 2012;45110:433–444.

[106] H JW. Ceramic stereolithography: additive manufacturing for ceramics by photopolymerization. Ann Rev Mater Res. 2016;46:19–40.

[107] Layani M, Wang X, Magdassi S. Novel materials for 3D printing by photopolymerization. Adv Mater. 2018;30(41):e1706344. doi:10.1002/adma.201706344

[108] Diesendruck CE, Sottos NR, Moore JS, et al. Biomimetic self-healing. Angew Chem Int Ed Engl. 2015;54(36):10428–10447. doi:10.1002/anie.201500484

[109] Sardon H, Dove AP. Plastics recycling with a difference. Science. 2018;360:380–381.

[110] Zhu G, Houck HA, Spiegel CA, et al. Introducing dynamic bonds in light-based 3D printing. Adv Funct Mater. 2023. doi:10.1002/adfm.202300456.

[111] Li X, Yu R, He Y, et al. Four-dimensional printing of shape memory polyurethanes with high strength and recyclability based on diels-alder chemistry. Polymer. 2020;200. doi:10.1016/j.polymer.2020.122532

[112] Song Y, Liu Y, Qi T, et al. Towards dynamic but super-tough healable polymers through biomimetic hierarchical hydrogen-bonding interactions. Angew Chem Int Ed Engl. 2018;57(42):13838–13842. doi:10.1002/anie.201807622

[113] Zhou X, Guo B, Zhang L, et al. Progress in bio-inspired sacrificial bonds in artificial polymeric materials. Chem Soc Rev. 2017;46(20):6301–6329. doi:10.1039/c7cs00276a

[114] Zhu G, Hou Y, Xiang J, et al. Digital light processing 3D printing of healable and recyclable polymers with tailorable mechanical properties. ACS Appl Mater Interfaces. 2021;13(29):34954–34961. doi:10.1021/acsami.1c08872

[115] Binyamin I, Grossman E, Gorodnitsky M, et al. 3D printing thermally stable high-performance polymers based on a dual curing mechanism. Adv Funct Mater. 2023;33:24. doi:10.1002/adfm.202214368

[116] Bobrin VA, Yao Y, Shi X, et al. Nano- to macro-scale control of 3D printed materials via polymerization induced microphase separation. Nat Commun. 2022;13(1):3577. doi:10.1038/s41467-022-31095-9

[117] Patel DK, Sakhaei AH, Layani M, et al. Highly stretchable and UV curable elastomers for digital light processing based 3D printing. Adv Mater. 2017;29:15. doi:10.1002/adma.201606000

[118] Cafiso D, Septevani AA, Noè C, et al. 3D printing of fully cellulose-based hydrogels by digital light processing. Sustain Mater Technol. 2022;32. doi:10.1016/j.susmat.2022.e00444

[119] Caprioli M, Roppolo I, Chiappone A, et al. 3D-printed self-healing hydrogels via digital light processing. Nat Commun. 2021;12(1):2462. doi:10.1038/s41467-021-22802-z

[120] EwaAndrzejewska. Photopolymerization kinetics of multifunctional monomers. Progr Polymer Sci. 2001;26(4):605–665. doi:10.1016/s0079-6700(01)00004-1.

[121] Crivello JV. The discovery and development of onium salt cationic photoinitiators. J Polymer Sci A Polymer Chem. 1999;37:4241–4254.

[122] Green WA. (2010). Industrial photoinitiators: a technical guide.

[123] Kaur M, Srivastava AK. Photopolymerization: a review. J Macromol Sci. 2002;42(4):481–512. doi:10.1081/mc-120015988

[124] Malik MS, Schlogl S, Wolfahrt M, et al. Review on UV-induced cationic frontal polymerization of epoxy monomers. Polymers (Basel). 2020;12:9. doi:10.3390/polym12092146.

[125] Sangermano M, Razza N, Crivello JV. Cationic UV-curing: technology and applications. Macromol Mater Eng. 2014;299(7):775–793. doi:10.1002/mame.201300349

[126] Green W. Green, W. A. Industrial Photoinitiators A Technical Guide; CRC.pdf, 2010.

[127] Fairbanks BD, Schwartz MP, Bowman CN, et al. Photoinitiated polymerization of PEG-diacrylate with lithium phenyl-2,4,6-trimethylbenzoylphosphinate: polymerization rate and cytocompatibility. Biomaterials. 2009;30(35):6702–6707. doi:10.1016/j.biomaterials.2009.08.055

[128] KT Nguyen JW. Photopolymerizable hydrogels for tissue engineering applications. Biomaterials. 2002;23 (22):4307–14. doi:10.1016/s0142-9612(02)00175-8.

[129] Arsu N, et al. One component thioxanthone based type II photoinitiators. Photochem UV Curing. 2006: 17–29.

[130] Zhang Y, Xu Y, Simon-Masseron A, et al. Radical photo-initiation with LEDs and applications in the 3D printing of composites. Chem Soc Rev. 2021;50(6):3824–3841. doi:10.1039/d0cs01411g

[131] Bryant SJ, Nuttelman CR, Anseth KS. Cytocompatibility of UV and visible light photoinitiating systems on cultured NIH/3T3 fibroblasts in vitro. J Biomater Sci Polym Ed. 2000;11(5):439–457. doi:10.1163/156856200743805

[132] Williams CG, Malik AN, Kim TK, et al. Variable cytocompatibility of six cell lines with photoinitiators used for polymerizing hydrogels and cell encapsulation. Biomaterials. 2005;26(11):1211–1218. doi:10.1016/j.biomaterials.2004.04.024

[133] Park S, Kim D, Ko SY, et al. Controlling uniformity of photopolymerized microscopic hydrogels. Lab Chip. 2014;14(9):1551–1563. doi:10.1039/c4lc00158c

[134] Pawar AA, et al. High-performance 3D printing of hydrogels by water-dispersible photoinitiator nanoparticles. Science Adv. 2016;2(4):e1501381.

[135] Huang X, Wang X, Zhao Y. Study on a series of water-soluble photoinitiators for fabrication of 3D hydrogels by two-photon polymerization. X. 2017;141:413–419. doi:10.1016/j.dyepig.2017.02.040.

[136] JR Choi KY, Choi JY, Cowie AC. Recent advances in photo-crosslinkable hydrogels for biomedical applications. BioTechniques. 2019;66(1):40–53. doi:10.2144/btn-2018-0083.

[137] Lin H, Zhang D, Alexander PG, et al. Application of visible light-based projection stereolithography for live cell-scaffold fabrication with designed architecture. Biomaterials. 2013;34(2):331–339. doi:10.1016/j.biomaterials.2012.09.048

[138] Wang Z, Kumar H, Tian Z, et al. Visible light photoinitiation of cell-adhesive gelatin methacryloyl hydrogels for stereolithography 3D bioprinting. ACS Appl Mater Interfaces. 2018;10(32):26859–26869. doi:10.1021/acsami.8b06607

[139] Kowsari K, Lee W, Yoo SS, et al. Scalable visible light 3D printing and bioprinting using an organic light-emitting diode microdisplay. iScience. 2021;24(11):103372. doi:10.1016/j.isci.2021.103372

[140] Zaborniak I CP. Ultrasound transducer array fabrication based on additive manufacturing of piezocomposites. Eur Polymer J. 2021;142:110152.

[141] Odent J, Wallin TJ, Pan W, et al. Highly elastic, transparent, and conductive 3D-printed ionic composite Hydrogels. Advanced Functional Materials. 2017;27(33). doi:10.1002/adfm.201701807.

[142] Gallastegui A, Dominguez-Alfaro A, Lezama L, et al. Fast visible-light photopolymerization in the presence of multiwalled carbon nanotubes: toward 3D printing conducting nanocomposites. ACS Macro Lett. 2022;11 (3):303–309. doi:10.1021/acsmacrolett.1c00758

[143] Kolczak U, et al. Reaction mechanism of monoacyl- and bisacylphosphine oxide photoinitiators studied by 31P-, 13C-, and 1H-CIDNP and ESR. J Amer Chem Soc. 1996;118(27):6477–6489. doi:10.1021/ja9534213.

[144] Vazquez-Martel C, Mainik P, Blasco E. Natural and naturally derived photoinitiating systems for light-based 3D printing. Organic Mater. 2022;4(04):281–291. doi:10.1055/a-1976-0453

[145] Kolb C, Lindemann N, Wolter H, et al. 3D-printing of highly translucent ORMOCER ®-based resin using light absorber for high dimensional accuracy. J Appl Polymer Sci. 2020;138:3. doi:10.1002/app.49691

[146] Wang F, Chong Y, Wang F, et al. Photopolymer resins for luminescent three-dimensional printing. J Appl Polymer Sci. 2017;134:32. doi:10.1002/app.44988

[147] Zhang R, Larsen NB. Stereolithographic hydrogel printing of 3D culture chips with biofunctionalized complex 3D perfusion networks. Lab Chip. 2017;17(24):4273–4282. doi:10.1039/c7lc00926g

[148] Stevens LJ, Burgess JR, Stochelski MA, et al. Amounts of artificial food dyes and added sugars in foods and sweets commonly consumed by children. Clin Pediatr (Phila). 2015;54(4):309–321. doi:10.1177/0009922814530803.

[149] Grigoryan B, DC Corbett SP, Sazer DW. Multivascular networks and functional intravascular topologies within biocompatible hydrogels. Science. 2019;364:458–464.

[150] Obaid MK, Abdullah LC, Idan IJ. Removal of reactive orange 16 Dye from aqueous solution by using modified kenaf core fiber. J Chem. 2016;2016:1–7. doi:10.1155/2016/4262578

[151] U Simon SD. Direct 3D printing of monolithic ion exchange adsorbers. J Chromatogr. 2019;1587:119–128. doi:10.1016/j.chroma.2018.12.017.

[152] Gong H, Bickham BP, Woolley AT, et al. Custom 3D printer and resin for 18 mu m×20 mu m microfluidic flow channels. Lab on a Chip. 2017;17:2899–2909. doi:10.1039/c7lc00644f

[153] Gastaldi M, Cardano F, Zanetti M, et al. Functional dyes in polymeric 3D printing: applications and perspectives. ACS Mater Lett. 2020;3(1):1–17. doi:10.1021/acsmaterialslett.0c00455

[154] Zhang Q, Bei HP, Zhao M, et al. Shedding light on 3D printing: printing photo-crosslinkable constructs for tissue engineering. Biomaterials. 2022b;286:121566. doi:10.1016/j.biomaterials.2022.121566

[155] Lee S, Kim Y, Park D, et al. The thermal properties of a UV curable acrylate composite prepared by digital light processing 3D printing. Compos Commun. 2021;26. doi:10.1016/j.coco.2021.100796

[156] Zhang B, Li H, Cheng J, et al. Mechanically robust and UV-curable shape-memory polymers for digital light processing based 4D printing. Adv Mater. 2021aa;27: e2101298. doi:10.1002/adma.202101298.

[157] Borrello J, Nasser P, Iatridis J, et al. 3D printing a mechanically-tunable acrylate resin on a commercial DLP-SLA printer. Addit Manuf. 2018;23:374–380. doi:10.1016/j.addma.2018.08.019

[158] He Y, Li N, Xiang Z, et al. Natural polyphenol as radical inhibitors used for DLP-based 3D printing of photosensitive gels. Mater Today Commun. 2022;33. doi:10.1016/j.mtcomm.2022.104698

[159] Tarcha PJ, Su L, Baker T, et al. Stability of photocurable anhydrides: methacrylic acid mixed anhydrides of nontoxic diacids. J Polymer Sci A Polymer Chem. 2001;39 (24):4189–4195. doi:10.1002/pola.10073

[160] Zhang X, Li Z, Yang P, et al. Polyphenol scaffolds in tissue engineering. Mater Horiz. 2021;8(1):145–167. doi:10.1039/d0mh01317j

[161] Russo A, Maschio G, Ampelli C. Reaction inhibition as a method for preventing thermal runaway in industrial processes. Macromol Symposia. 2007;259(1):365–370. doi:10.1002/masy.200751341

[162] Esfandiari P, Ligon SC, Lagref JJ, et al. Efficient stabilization of thiol-ene formulations in radical photopolymerization. J Polymer Sci A Polymer Chem. 2013;51 (20):4261–4266. doi:10.1002/pola.26848

[163] Salas A, Zanatta M, Sans V, et al. Chemistry in light-induced 3D printing. ChemTexts. 2023b;9:1. doi:10.1007/s40828-022-00176-z

[164] Nauman N, Zaquen N, Boyer C, et al. Miniemulsion photopolymerization in a continuous tubular reactor: particle size controlviamembrane emulsification. Polymer Chem. 2020;11(28):4660–4669. doi:10.1039/d0py00654h

[165] Davidson RS. Exploring the science,: technology and applications of UV and EB curing. Sita Technology. 1999.

[166] Fouassier J-P. (1995). Photoinitiation, photopolymerization, and photocuring: fundamentals and applications.

[167] Fouassier J-P, Rabek JF. *Radiation curing in polymer science and technology: practical aspects and applications*. Springer Science & Business Media; 1993.

[168] Sato R, Kurihara T, Takeishi M. Rate enhancement of amines in the photopolymerization of methyl methacrylate under oxygen. Polymer International. 1998;47 (2):159–164.

[169] Decker C. Die Makromolekulare Chemie. 1979;180 (8):2027–2030. doi:10.1002/macp.1979.021800818

[170] Belon C, Allonas X, Croutxé-barghorn C, et al. Overcoming the oxygen inhibition in the photopolymerization of acrylates: A study of the beneficial effect of triphenylphosphine. J Polymer Sci A Polymer Chem. 2010;48(11):2462–2469. doi:10.1002/pola.24017

[171] Ligon SC, Husar B, Wutzel H, et al. Strategies to reduce oxygen inhibition in photoinduced polymerization. Chem Rev. 2014;114(1):557–589. doi:10.1021/cr3005197

[172] Yong He QG, Jin Y. (2022). *Cell assembly with 3D bioprinting*. WILEY-VCH.

[173] Kim SH, Yeon YK, Lee JM, et al. Precisely printable and biocompatible silk fibroin bioink for digital light processing 3D printing. Nat Commun. 2018;9(1):1620. doi:10.1038/s41467-018-03759-y

[174] Mendes-Felipe C, Oliveira J, Etxebarria I, et al. State-of-the-Art and future challenges of UV curable polymer-based smart materials for printing technologies. Adv Mater Technol. 2019;4:3. doi:10.1002/admt.201800618

[175] Wang S, Yin J, Huang W, et al. UV-induced disulfide metathesis: strengthening interlayer adhesion and rectifying warped 3D printed materials. Addit Manufac. 2022;59. doi:10.1016/j.addma.2022.103085

[176] Xu X, Zhou S, Wu J, et al. Relationship between the adhesion properties of UV-curable alumina suspensions and the functionalities and structures of UV-curable acrylate monomers for DLP-based ceramic stereolithography. Ceramics Int. 2021;47(23):32699–32709. doi:10.1016/j.ceramint.2021.08.166

[177] Song P, Li M, Zhang B, et al. DLP fabricating of precision GelMA/HAp porous composite scaffold for bone tissue engineering application. Composites B Eng. 2022;244. doi:10.1016/j.compositesb.2022.110163

[178] Weng Z, Huang X, Peng S, et al. 3D printing of ultra-high viscosity resin by a linear scan-based vat photopolymerization system. Nat Commun. 2023;14(1):4303. doi:10.1038/s41467-023-39913-4

[179] Wu L, Dong Z. Interfacial regulation for 3D printing based on slice-based photopolymerization. Adv Mater. 2023;35(29):e2300903. doi:10.1002/adma.202300903

[180] Raj R, Dixit AR, Singh SS, et al. Print parameter optimization and mechanical deformation analysis of alumina-nanoparticle doped photocurable nanocomposites fabricated using vat-photopolymerization based additive technology. Addit Manufac. 2022;60. doi:10.1016/j.addma.2022.103201

[181] Yu B, Zheng J, Wu J, et al. Preparation of isotropic tensile photosensitive resins for digital light processing 3D printing using orthogonal thiol-ene and thiol-epoxy dual-cured strategies. Polymer Testing. 2022;116. doi:10.1016/j.polymertesting.2022.107767

[182] Bae JH, Won JC, Lim WB, et al. Highly flexible and photo-activating acryl-polyurethane for 3D steric architectures. Polymers (Basel. 2021;13:6. doi:10.3390/polym13060844.

[183] Hanon MM, Ghaly A, Zsidai L, et al. Tribological characteristics of digital light processing (DLP) 3D printed graphene/resin composite: influence of graphene presence and process settings. Mater Design. 2022;218. doi:10.1016/j.matdes.2022.110718

[184] Yu C, Schimelman J, Wang P, et al. Photopolymerizable biomaterials and light-based 3D printing strategies for biomedical applications. Chem Rev. 2020;120 (19):10695–10743. doi:10.1021/acs.chemrev.9b00810

[185] Karalekas D, Aggelopoulos A. Study of shrinkage strains in a stereolithography cured acrylic photopolymer resin. J Mater Process Technol. 2003;136(1–3):146–150. doi:10.1016/s0924-0136(03)00028-1

[186] Salmoria GV, Ahrens CH, Beal VE, et al. Evaluation of post-curing and laser manufacturing parameters on the properties of SOMOS 7110 photosensitive resin used in stereolithography. Mater Design. 2009;30 (3):758–763. doi:10.1016/j.matdes.2008.05.016

[187] Steyrer B, Busetti B, Harakály G, et al. Hot lithography vs. room temperature DLP 3D-printing of a dimethacrylate. Addit Manufac. 2018;21:209–214. doi:10.1016/j.addma.2018.03.013

[188] Eibel A, Fast DE, Gescheidt G. Choosing the ideal photoinitiator for free radical photopolymerizations: predictions based on simulations using established data. Polymer Chemistry. 2018;9(41):5107–5115. doi:10.1039/c8py01195h

[189] Weigel N, Mannel MJ, Thiele J. Flexible materials for high-resolution 3D printing of microfluidic devices with integrated droplet size regulation. ACS Appl Mater Interface. 2021;26:31086–31101. doi:10.1021/acsami.1c05547

[190] Taki K, Watanabe Y, Ito H, et al. Effect of oxygen inhibition on the kinetic constants of the UV-radical photopolymerization of diurethane dimethacrylate/photoinitiator systems. Macromolecules. 2014;47 (6):1906–1913. doi:10.1021/ma402437q

[191] Yang Y, Zhang Q, Xu T, et al. Photocrosslinkable nanocomposite ink for printing strong,: biodegradable and bioactive bone graft. Biomaterials. 2020;263:120378. doi:10.1016/j.biomaterials.2020.120378

[192] Andrzejewska E. Free radical photopolymerization of multifunctional Monomers. In: *Three-dimensional microfabrication using two-photon polymerization*. 2016. p. 62–81.

[193] Dickens SH, et al. Photopolymerization kinetics of methacrylate dental resins. Macromolecules. 2003;36 (16):6043–6053.

[194] Bucciarelli, A., Paolelli, X., De Vitis, E., et al. VAT photopolymerization 3D printing optimization of high aspect ratio structures for additive manufacturing of chips towards biomedical applications. Addit Manufac. 2022;60; doi:10.1016/j.addma.2022.103200

[195] Razavi Bazaz S, Rouhi O, Raoufi MA, et al. 3D printing of inertial microfluidic devices. Sci Rep. 2020;1:5929. doi:10.1038/s41598-020-62569-9

[196] Yuan C, Kowsari K, Panjwani S, et al. Ultrafast three-dimensional printing of optically smooth microlens arrays by oscillation-assisted digital light processing. ACS Appl Mater Interfaces. 2019;11(43):40662–40668. doi:10.1021/acsami.9b14692

[197] Streets AM, Huang Y. Chip in a lab: microfluidics for next generation life science research. Biomicrofluidics. 2013;7 (1):11302. doi:10.1063/1.4789751

[198] Zhang H, Liu H, Zhang N. A review of microinjection moulding of polymeric micro devices. Micromachines (Basel). 2022;13:9. doi:10.3390/mi13091530.

[199] Guo MT, Rotem A, Heyman JA, et al. Droplet microfluidics for high-throughput biological assays. Lab Chip. 2012;12(12):2146–2155. doi:10.1039/c2lc21147e

[200] Son J, Samuel R, Gale BK, et al. Separation of sperm cells from samples containing high concentrations of white blood cells using a spiral channel. Biomicrofluidics. 2017;11(5):054106. doi:10.1063/1.4994548

[201] Jafek AR, Harbertson S, Brady H, et al. Instrumentation for xPCR incorporating qPCR and HRMA. Anal Chem. 2018;90(12):7190–7196. doi:10.1021/acs.analchem.7b05176

[202] Whitesides GM. The origins and the future of microfluidics. Nature. 2006;442(7101):368–373. doi:10.1038/nature05058

[203] Kim P, Lee SE, Jung HS, et al. Soft lithographic patterning of supported lipid bilayers onto a surface and inside microfluidic channels. Lab Chip. 2006;6(1):54–59. doi:10.1039/b512593f

[204] Yazdi AA, Popma A, Wong W, et al. 3D printing: an emerging tool for novel microfluidics and lab-on-a-chip applications. Microfluid Nanofluid. 2016;20:3. doi:10.1007/s10404-016-1715-4

[205] Hongbin Y, Guangya Z, Siong CF, et al. Novel polydimethylsiloxane (PDMS) based microchannel fabrication method for lab-on-a-chip application. Sensors Actuat B Chem. 2009;137(2):754–761. doi:10.1016/j.snb.2008.11.035

[206] Wilson ME, Kota N, Kim Y, et al. Fabrication of circular microfluidic channels by combining mechanical micromilling and soft lithography. Lab Chip. 2011;11 (8):1550–1555. doi:10.1039/c0lc00561d

[207] Mao M, He J, Li X, et al. The emerging frontiers and applications of high-resolution 3D printing. Micromachines, Micro/Nano Manufacturing Backgroud. 2017;4. doi:10.3390/mi8040113.

[208] Zhu W, Qu X, Zhu J, et al. Direct 3D bioprinting of prevascularized tissue constructs with complex microarchitecture. Biomaterials. 2017: 106–115. doi:10.1016/j.biomaterials.2017.01.042

[209] Shallan AI, Smejkal P, Corban M, et al. Cost-effective three-dimensional printing of visibly transparent microchips within minutes. Anal Chem. 2014;6:3124–3130. doi:10.1021/ac4041857

[210] Buttner U, Sivashankar S, Agambayev S, et al. Flash µ-fluidics: a rapid prototyping method for fabricating microfluidic devices. RSC Adv Microfluidic Chip. 2016;78:74822–74832. doi:10.1039/c6ra13582j.

[211] Macdonald NP, Cabot JM, Smejkal P, et al. Comparing microfluidic performance of three-dimensional (3D) printing platforms. Anal Chem. 2017;7:3858–3866. doi:10.1021/acs.analchem.7b00136

[212] van der Linden P, Popov AM, Pontoni D. Accurate and rapid 3D printing of microfluidic devices using wavelength selection on a DLP printer. Lab Chip. 2020;22:4128–4140. doi:10.1039/d0lc00767f.

[213] Bhusal A, Dogan E, Nguyen HA, et al. Multi-material digital light processing bioprinting of hydrogel-based microfluidic chips. Biofabrication. 2021;1. doi:10.1088/1758-5090/ac2d78.

[214] Limaye AS, Rosen DW. Process planning method for mask projection micro-stereolithography. Rapid Prototyping Journal. 2007;13(2):76–84. doi:10.1108/13552540710736759.

[215] Zhou C, Chen Y, Waltz RA. Optimized mask image projection for solid freeform fabrication. In: *Paper presented at the international design engineering technical conferences and computers and information in engineering conference.* 2009.

[216] Gong H, Woolley AT, Nordin GP. High density 3D printed microfluidic valves: pumps, and multiplexers. Lab Chip. 2016;16(13):2450–2458. doi:10.1039/c6lc00565a

[217] Männel MJ, Selzer L, Bernhardt R, et al. Optimizing process parameters in commercial micro-stereolithography for forming emulsions and polymer microparticles in nonplanar microfluidic devices. Adv Mater Technol. 2019;4:1. doi:10.1002/admt.201800408

[218] Kuo AP, Bhattacharjee N, Lee YS, et al. High-Precision stereolithography of biomicrofluidic devices. Adv Mater Technol. 2019;4:6. doi:10.1002/admt.201800395

[219] Lee YS, Bhattacharjee N, Folch A. 3D-printed Quake-style microvalves and micropumps. Lab Chip. 2018;18 (8):1207–1214. doi:10.1039/C8LC00001H

[220] Xu Y, Qi F, Mao H, et al. In-situ transfer vat photopolymerization for transparent microfluidic device

fabrication. Nat Commun. 2022;13(1):918. doi:10.1038/s41467-022-28579-z

[221] Cui K., et al. A kind of accuracy improving method based on error analysis and feedback for DLP 3D Printing. In 2019 IEEE international conference on service operations and logistics, and informatics (SOLI), IEEE, 2019. Retrieved from Dsitoration

[222] Huang YC, Pan JW. High contrast ratio and compact-sized prism for DLP projection system. Opt Express. 2014;22(14):17016–17029. doi:10.1364/OE.22.017016

[223] Pan JW, Wang HH. High contrast ratio prism design in a mini projector. Appl Opt. 2013;52(34):8347–8354. doi:10.1364/AO.52.008347

[224] Zhen Chen GX, Ju K, et al. Study on mask graphics optimization of face exposure rapid prototyping system. Mechatronics. 2016;22(1):23–28.

[225] Li Z, Chen Z, Liu J, et al. Additive manufacturing of lightweight and high-strength polymer-derived SiOC ceramics. Virtual Phys Protot. 2020;15(2):163–177. doi:10.1080/17452759.2019.1710919

[226] Li Y, Mao Q, Yin J, et al. Theoretical prediction and experimental validation of the digital light processing (DLP) working curve for photocurable materials. Addit Manufac. 2021. doi:10.1016/j.addma.2020.101716.

[227] Smith JM. Motorized stage DLP large-scale printing: U.S. Patent No. 6, 245. 21 May 2002, 2002.

[228] Mitcham L, Nelson WE. Multi-projector printing: U.S. Patent 5, 180, 1993.

[229] Wu C. et al. Delta DLP 3D printing with large size. IEEE/RSJ international conference on intelligent robots and systems (IROS). IEEE, 2016.

[230] Zheng X, Smith W, Jackson J, et al. Multiscale metallic metamaterials. Nat Mater. 2016;10:1100–1106. doi:10.1038/nmat4694

[231] Sack J-R and Urrutia J. Handbook of computational geometry, 1999.

[232] Xu Y, Mao H, Liu C, et al. Hopping light Vat photopolymerization for multiscale fabrication. Small. 2023;19 (11):e2205784. doi:10.1002/smll.202205784

[233] Ryan Wicker FM, Elkins C. Multiple material micro-fabrication extending stereo lithography to tissue engineering and other novel application, 2004.

[234] Han D, Yang C, Fang NX, et al. Rapid multi-material 3D printing with projection micro-stereolithography using dynamic fluidic control. Additive Manuf. 2019;27:606–615. doi:10.1016/j.addma.2019.03.031

[235] Martin JJ, Fiore BE, Erb RM. Designing bioinspired composite reinforcement architectures via 3D magnetic printing. Nat Commun. 2015;6:8641. doi:10.1038/ncomms9641

[236] Yang Y, Chen Z, Song X, et al. Biomimetic anisotropic reinforcement architectures by electrically assisted nanocomposite 3D printing. Adv Mater. 2017;29:11. doi:10.1002/adma.201605750

[237] Cheng J, Wang R, Sun Z, et al. Centrifugal multimaterial 3D printing of multifunctional heterogeneous objects. Nat Commun. 2022;13(1):7931. doi:10.1038/s41467-022-35622-6

[238] Toombs, J. T., et al. Volumetric additive manufacturing of silica glass with microscale computed axial lithography. Science. 2022;376:308–312.

[239] Regehly M, Garmshausen Y, Reuter M, et al. Xolography for linear volumetric 3D printing. Nature. 2020;588(7839):620–624. doi:10.1038/s41586-020-3029-7

[240] De Beer, MP, et al. Rapid, continuous additive manufacturing by volumetric polymerization inhibition patterning. Science Advances, 2019, 8723.